Neuroscience

Eye-specific differences in active zone addition during synaptic competition in the developing visual system

Chenghang Zhang, Tarlan Vatan, Colenso M Speer

Department of Biology, University of Maryland, College Park, College Park, United States 20742

Reviewed Preprint
v4 • October 24, 2025
Revised by authors

Reviewed Preprint
v3 • September 8, 2025

Reviewed Preprint
v2 • December 16, 2024

Reviewed Preprint
v1 • October 23, 2023

eLife Assessment

This is a **valuable** analysis of STORM data that characterizes the clustering of active zones in retinogeniculate terminals across ages and in the absence of retinal waves. The design makes it possible to relate fixed time point structural data to a known outcome of activity-dependent remodeling. The latest revision has tempered the causal claims made in previous versions. The result provides **solid** structural support for the hypotheses regarding how activity influences the clustering of these synapses.

https://doi.org/10.7554/eLife.91431.4.sa2

Abstract

Spatially clustered synaptic inputs enable local dendritic computations important for learning, memory, and sensory processing. In the mammalian visual system, individual retinal ganglion cell (RGC) axons form clustered terminal boutons containing multiple active zones onto relay cell dendrites in the dorsal lateral geniculate nucleus (dLGN). This mature architecture arises through the addition of release sites, which strengthens selected afferents while weaker inputs are pruned. Following eye-opening, spontaneous activity and visual experience promote synaptic refinement and bouton clustering after binocular inputs have segregated. However, anatomical changes in release site addition and spatial patterning during earlier stages of eye-specific competition are not well understood. To investigate this, we examined the spatial organization of eye-specific active zones in wild type mice and a mutant line with disrupted cholinergic retinal waves. Using volumetric super-resolution single-molecule localization microscopy and electron microscopy, we found that individual retinogeniculate boutons begin forming multiple nearby presynaptic active zones during the first postnatal week. Both eyes generate these “multi-active-zone” (mAZ) inputs throughout refinement, but the dominant-eye forms more numerous mAZ contacts, each with more active zones and larger vesicle pools. At the height of competition (postnatal day 4), the non-dominant-eye projection adds many single active zone (sAZ) synapses. Mutants with abnormal cholinergic retinal waves still form mAZ inputs, but develop fewer synapses overall and show reduced synaptic clustering in projections from both eyes. Together, these findings reveal eye-specific differences in release site addition that correlate with axonal refinement outcomes during retinogeniculate refinement.

Introduction

A key mechanism for neuronal signal processing is the formation of spatially clustered synapses that facilitate local computations within individual dendrites [1–3]. Through biophysical signal integration mechanisms, neighboring synaptic inputs play critical computational roles in learning, memory, and sensory processing underlying cognition and behavior [4–7]. During circuit development, both spontaneous and sensory-driven neural activity regulate synaptic clustering, stabilizing some synapses and eliminating others to establish mature connectivity patterns [6–8].

The refinement of retinal inputs to the dorsal lateral geniculate nucleus (dLGN) of the thalamus is a model example of activity-dependent synaptic clustering [9]. Over development, boutons within the terminal arbors of individual retinogeniculate axons cluster progressively [10–13], creating multiple synaptic contacts onto individual postsynaptic targets [14–16]. Concurrently, developing RGC boutons add presynaptic release sites such that some mature retinogeniculate terminals contain several dozen active zones (AZs) [16, 17]. The formation of clustered boutons with multiple release sites subserves a critical “driver” function of retinogeniculate input [18, 19].

Retinogeniculate bouton clustering depends on visual experience, and dark-rearing after eye-opening reduces clustering within individual axon arbors [12]. However, less is known about synaptic spatial relationships and activity-dependent release site refinement during eye-specific competition before eye-opening. During early axon ingrowth, individual RGCs extend sparse side branches in the incorrect eye-specific territory [20–22]. These transient branches form synapses that contain fewer presynaptic vesicles than those made by the same axon in the correct eye-specific domain [23]. Functional recordings after eye-opening show that while many RGC inputs are pruned, the remaining inputs strengthen by adding release sites [24]. This leads to glutamate spillover and cross talk between RGC inputs that increases postsynaptic relay neuron excitability [25]. Thus, early eye-specific differences in release site number or spacing may contribute to binocular input refinement prior to eye-opening.

In a previous study from our laboratory, we used volumetric stochastic optical reconstruction microscopy (STORM), anterograde tract tracing, and immunohistochemical labeling of synaptic proteins to show that dominant-eye synapses contain more total vesicles and have more vesicles near the AZ (putative docking) compared with non-dominant-eye synapses [26]. However, we did not examine whether eye-specific inputs differ in AZ number or AZ spatial proximity (clustering) during synaptic competition. To address this gap, we reanalyzed our published dataset, focusing on eye-specific AZ spatial relationships. We found that projections from each eye form a subset of retinogeniculate inputs in which several (2-4) AZs share a common cluster of presynaptic vesicles. We refer to these synapses as multi-active-zone (mAZ) inputs. All other retinogeniculate inputs contained one single active zone and its associated vesicle cluster, and we term these single-active-zone (sAZ) synapses.

During eye-specific synaptic competition, the dominant-eye projection formed more mAZ inputs, each with more AZs and a larger presynaptic vesicle pool compared to the non-dominant eye projection. Similarly, the dominant-eye had higher vesicle signal at sAZ inputs. At the peak of synaptic competition midway through the first postnatal week (postnatal day 4), the non-dominant-eye formed numerous sAZ inputs, equalizing the global synapse density between the two eyes. These eye-specific AZ patterns were disrupted in a mutant mouse line with abnormal stage II cholinergic retinal waves and retinogeniculate segregation defects.

Results

Retinogeniculate inputs form multiple active zones during eye-specific competition

To investigate active zone refinement during eye-specific segregation, we reanalyzed a volumetric super-resolution imaging dataset previously published by our laboratory [26]. We used volumetric STochastic Optical Reconstruction Microscopy (STORM) [27] to image the dLGNs of wild-type (WT) mice at three postnatal ages (P2, P4, and P8) (**Fig. 1A**). We labeled eye-specific inputs by monocular injection of Alexa Fluor-conjugated cholera toxin subunit B tracer (CTB) together with immunostaining for presynaptic Bassoon, postsynaptic Homer1, and presynaptic vesicular glutamate transporter 2 (VGluT2) proteins (**Fig. 1B**). We collected separate image volumes (~45K μm^3 each) from three biological replicates at each age. To assess the impact of spontaneous retinal activity on synaptic development across the same time period, we performed identical experiments in β2-knockout (β2KO) mice lacking the beta 2 subunit of the nicotinic acetylcholine receptor, a mutation that disrupts spontaneous cholinergic retinal wave activity, eye-specific segregation, and retinogeniculate synapse development [22, 26, 28–36] (**Fig. 1A**). Because eye-specific segregation is incomplete until ~P8, we limited our re-analysis to the future contralateral eye-specific region of the dLGN, which is reliably identified across all stages of postnatal development (**Fig. 1A**, see also Materials and Methods).

By analyzing synapses in the contralateral dLGN from eighteen mice across three ages and two genotypes (Table S1), STORM revealed two classes of retinogeniculate inputs distinguished by active zone (AZ) number (**Fig. 1B**). We defined each retinogeniculate input as a single contiguous VGluT2 cluster together with all its associated presynaptic (Bassoon) and postsynaptic (Homer1) paired synaptic labels. Using this definition, inputs that had multiple (2-4) Bassoon AZs were classified as multi-active-zone (mAZ) inputs, while those with a single Bassoon AZ were designated single-active-zone (sAZ) inputs (**Fig. 1B**). Most mAZ inputs contained two AZs (~70-90%, varying with age, genotype, and eye-of-origin); smaller proportions contained three AZs (~10-20%) or four or more AZs (<5%) (Table S1).

Each mAZ input could be a single terminal bouton with several AZs, or a cluster of sAZ synapses within separate boutons [10, 11, 15, 16, 37]. To address this, we used electron microscopy (EM) to image retinogeniculate terminals in the dLGN at P8. We generated a transgenic line expressing mitochondrial matrix-targeted dimeric dAPEX2 reporter [38] in ipsilaterally-projecting RGCs [39–41], providing unambiguous mitochondrial labeling in ipsiRGC axons. EM images confirmed the presence of individual retinogeniculate boutons with multiple active zones, consistent with our STORM data (**Fig. 1C**). Previous EM reconstructions of retinogeniculate inputs reported no evidence of RGC bouton convergence at the end of the first postnatal week [11]. Together, these results suggest that mAZ inputs in STORM images are single RGC terminals that house several closely spaced release sites. Hereafter, we use the word “synapse” only to refer to each partnered active zone (Bassoon/Homer1 pairs); mAZ inputs contain several synapses, while each sAZ input is one synapse.

Changes in eye-specific input density during synaptic competition

In our previous analysis, we reported global eye-specific synapse densities that reflected the combined mAZ and sAZ inputs. Dominant-eye synapse density was greater than that of the non-dominant eye at P2 and P8, but eye-specific synapse densities were equivalent at P4 during the peak of synaptic competition [26]. To determine how these two input classes evolve during competition, we quantified the densities and percentages of mAZ and sAZ inputs in WT and β2KO mice (**Fig. 2A**). Eye-of-origin for each retinogeniculate input was assigned by colocalizing CTB

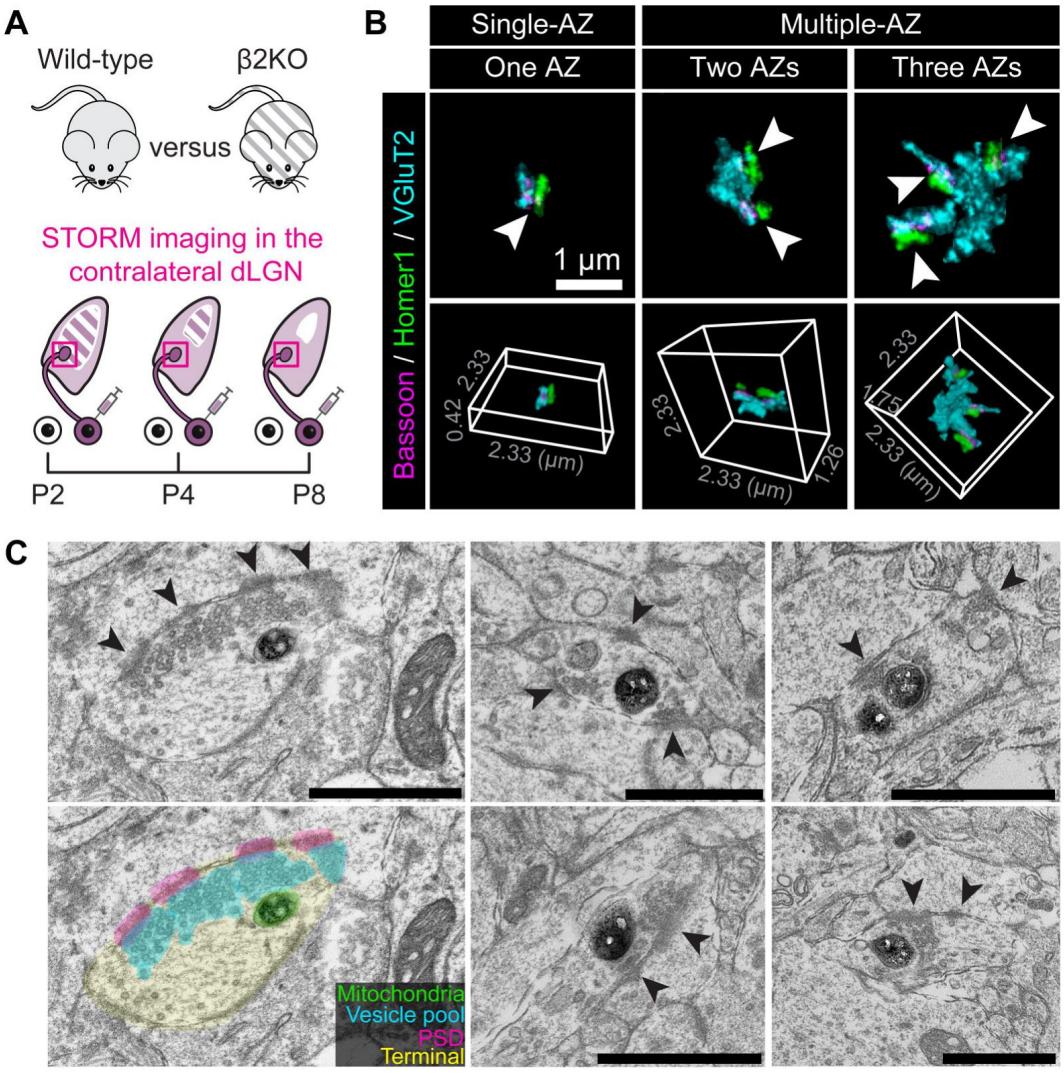

Fig. 1

Retinogeniculate boutons form multiple active zones during eye-specific competition

(A) Experimental design. CTB-Alexa 488 was injected into the right eye of wild-type and β2KO mice. One day after the treatment, tissue was collected from the left dLGN at P2, P4, and P8. Red squares indicate the STORM imaging regions that were analyzed. (B) Representative examples of individual sAZ and mAZ inputs, with corresponding active zone counts ranging from one to three. Upper panels show Z-projections of inputs and lower panels show the corresponding 3D volume. Arrowheads point to individual Bassoon clusters (active zones) paired with postsynaptic Homer1 labels within each input. All examples are from a WT P8 sample. (C) Electron micrographs of mAZ retinogeniculate inputs in a P8 $ET33^{Cre}$::$ROSA26^{LSL\text{-}Matrix\text{-}dAPEX2}$ mouse. Darkly-stained dAPEX2(+) mitochondria are present within ipsilaterally-projecting RGC terminals. Arrowheads point to electron-dense material at the postsynaptic density, apposed to individual active zones with clustered presynaptic synaptic vesicles.

signal with VGluT2 (**Fig. 2B**). Binocular CTB control injections showed that anterograde tracing labeled >97% of retinogeniculate synapses at P4 and P8, ensuring accurate eye-specific assignment [26]. Within the contralateral eye-specific region of the dLGN, CTB(+) VGluT2 clusters were classified as "dominant-eye" inputs and CTB(-) VGluT2 clusters as "non-dominant eye" inputs (**Fig. 2B**).

After false discovery rate (FDR) correction for multiple comparisons within each age and genotype (see Quantification and Statistical Analysis; p(adj) values shown in all figures and Table S2), we found that the density of CTB(+) mAZ inputs tended to be higher than CTB(-) mAZ inputs in WT mice (**Fig. 2C**, top left). Consistent with this trend, the mAZ input fraction (% of all inputs) was significantly higher for CTB(+) dominant-eye inputs at P4 and P8 (Fig. S1, top). β2KO mice also developed differences in mAZ input density favoring the dominant-eye (**Fig. 2C**, bottom left; Fig. S1, bottom). For WT sAZ synapses, the dominant-eye had a significantly higher synapse density at P2 [p(adj)=0.026, Cohen's d = 5.31] and trended higher at P8 [p(adj)=0.072, Cohen's d = 2.73]. At P4, however, sAZ synapse density was equivalent between the eyes (**Fig. 2C**, top right; Table S2/S3). This pattern resulted from non-dominant eye sAZ synapse addition, which equalized the global input density between the eyes at P4 as we reported previously (5/95% confidence interval, -0.014-0.011 synapses / μm^3). In β2KO mice at P4, the non-dominant eye formed fewer sAZ synapses (**Fig. 2C**, bottom right; see Tables S2/S3). Thus, β2KO mice with disrupted retinal activity maintain a higher mAZ input fraction in the dominant-eye projection, but sAZ synapse addition is reduced at the peak of competition.

Multi- and single-active-zone inputs from the dominant eye show increased vesicle pool size and vesicle proximity to the active zone

We previously reported a dominant-eye bias in VGluT2 volume when considering all retinogeniculate inputs [26]. Here, we assessed presynaptic maturation separately in sAZ and mAZ inputs by measuring their total VGluT2 volume. In WT mice, both mAZ (**Fig. 3A**, left) and sAZ (**Fig. 3B**, left) inputs showed significant eye-specific volume differences in the middle of eye-specific competition at P4. At this age in WT mice, the median VGluT2 cluster volume in dominant-eye mAZ inputs was ~3.55 ± 1.3 μm^3 larger (mean ± S.E.) than that of non-dominant-eye inputs (**Fig. 3A**, left). In contrast, β2KO mice showed a smaller ~1.9 ± 1.1 μm^3 (mean ± S.E.) volume difference between median eye-specific mAZ inputs at the same age (**Fig. 3A**, right panel). For sAZ synapses at P4, the magnitudes of eye-specific differences in median VGluT2 volume (mean ± S.E.) were ~2.1 ± 1.0 μm^3 in WT (**Fig. 3B**, left) and ~1.5 ± 1.1 in β2KO mice (**Fig. 3B**, right). Thus, both mAZ and sAZ vesicle pool volumes are larger for the dominant eye, with the largest eye-specific differences seen for mAZ inputs in WT mice (see Table S3).

In addition to total vesicle pool volume, we quantified the readily releasable pool by measuring VGluT2 volume within a 70 nm shell around each AZ, considering this a proxy for docked vesicles (Fig. S2A-C) [26]. In WT mice at P4, dominant-eye inputs showed greater vesicle volume per AZ than non-dominant inputs, in both mAZ and sAZ terminals (Fig. S2B, left; Table S3). These eye-specific differences were absent in β2KO mice (Fig. S2B, right; Table S3). However, when comparing mAZ and sAZ inputs from the same eye, vesicle volume per AZ was similar across all ages and genotypes (Fig. S2A-C; Table S2). This confirms our previous finding that vesicle docking favors the dominant-eye [26] and shows that AZs formed by a single eye have similar docking levels in both their mAZ and sAZ terminals.

Vesicle pool size scales with active zone number

Because mAZ inputs showed greater total VGluT2 volume than sAZ synapses, yet exhibited comparable vesicle docking, the disparity could reflect a scaling effect of vesicle pool size with increased AZ number. To evaluate how presynaptic vesicle pool volume scales with AZ number, we compared the Bassoon cluster number to VGluT2 volume for every retinogeniculate input. In both WT (Fig. S2D) and β2KO mice (Fig. S2E), mAZ inputs contained an average of 2-3 Bassoon

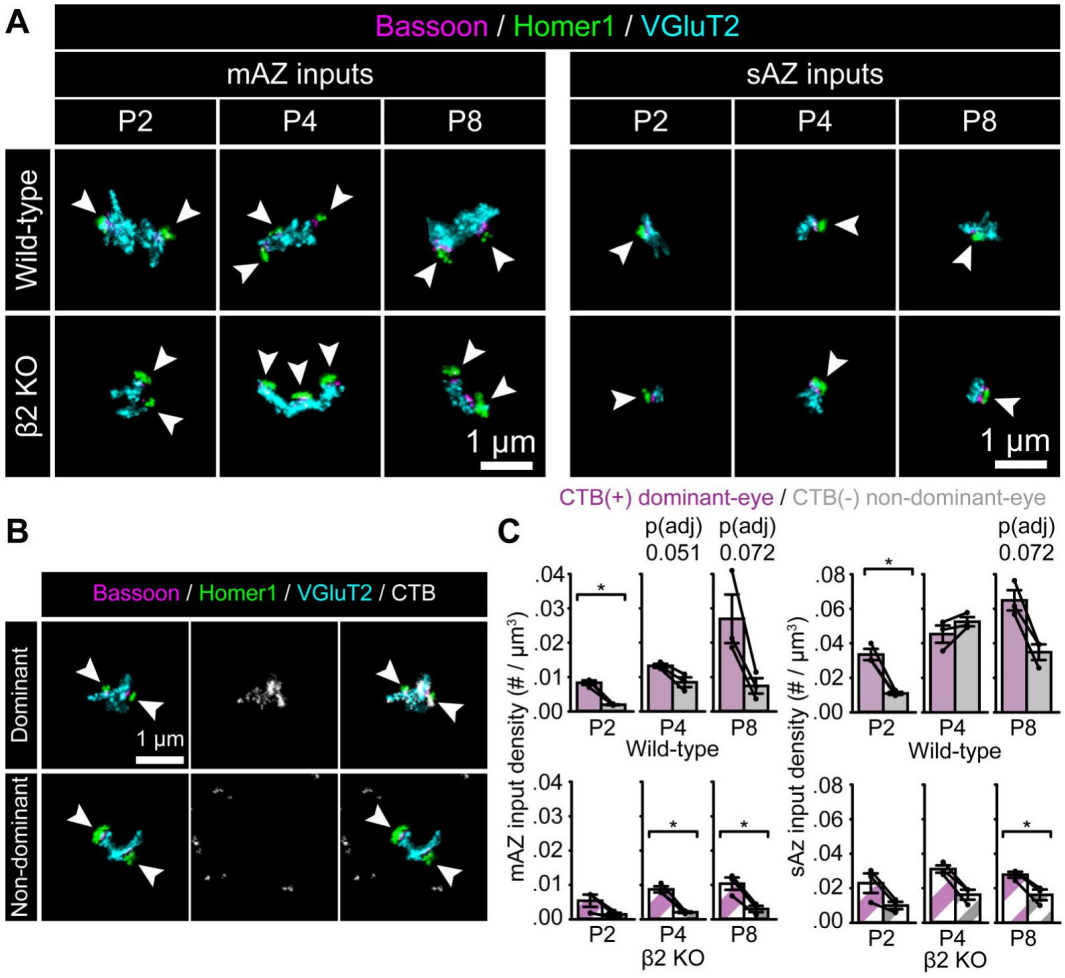

Fig. 2

Changes in eye-specific input density during synaptic competition

(A) Representative Z-projection images of mAZ and sAZ inputs across ages and genotypes. Arrowheads point to individual Bassoon/Homer1 cluster pairs indicating release sites. (B) Representative CTB(+) dominant-eye (top panels) and CTB(-) non-dominant-eye (bottom panels) mAZ inputs in a WT P8 sample, showing synaptic (left panels), CTB (middle panels), and merged labels (right panels). Arrowheads point to individual Bassoon/Homer1 paired clusters. (C) Eye-specific mAZ (left) and sAZ (right) input density across development in WT (top panels) and β2KO mice (bottom panels). Black dots represent mean values from separate biological replicates and black lines connect eye-specific measurements within each replicate (N=3 for each age and genotype). Error bars represent group means ± SEMs. Statistical significance between eye-specific measurements was assessed for each genotype using two-tailed paired T-tests with Benjamini-Hochberg FDR correction (α = 0.05) at each age. *p(adj)<0.05.

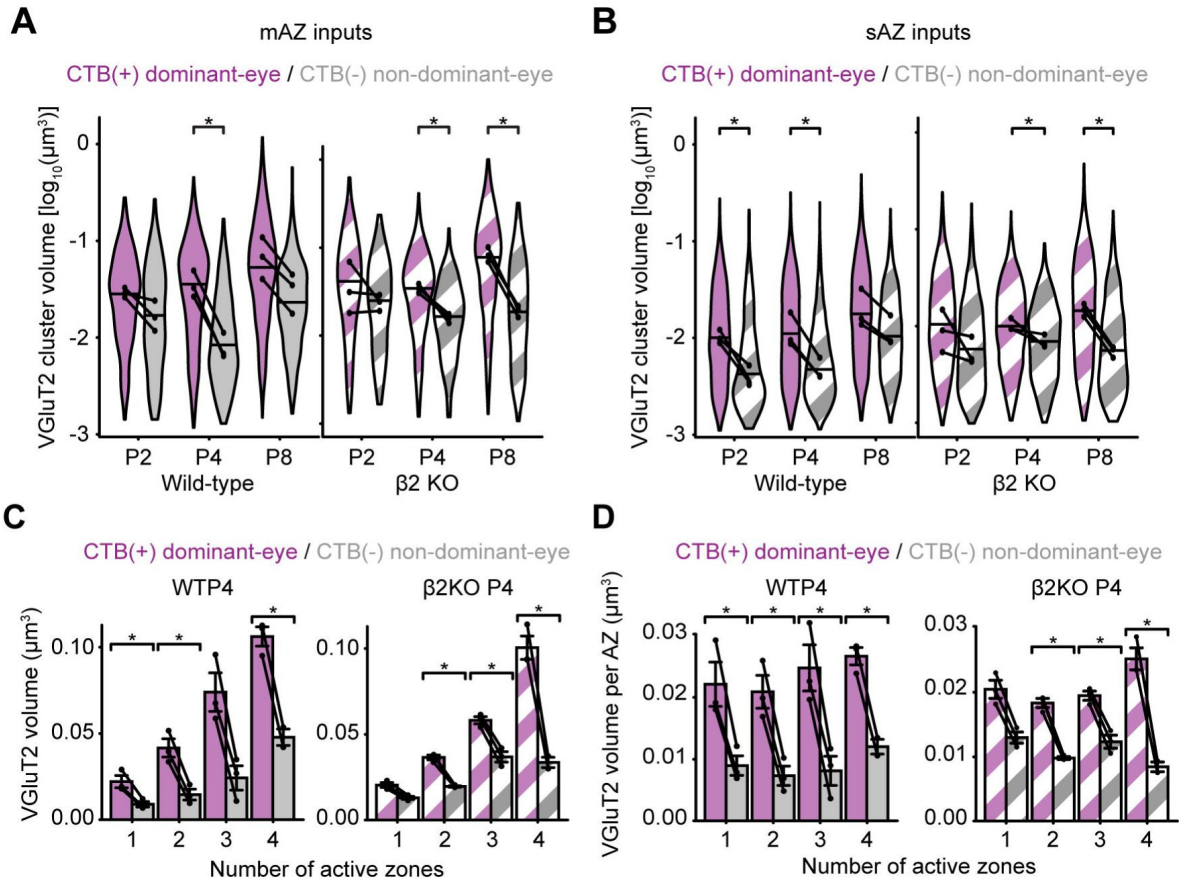

Fig. 3

Dominant-eye inputs show larger vesicle pools that scale with active zone number

(A and B) Violin plots showing the distribution of VGluT2 cluster volume for (A) mAZ and (B) sAZ inputs in WT (filled) and β2KO mice (striped) at each age. The width of each violin plot reflects the relative synapse proportions across the entire grouped data set at each age (N=3 biological replicates) and the maximum width was normalized across all groups. The black dots represent the median value of each biological replicate (N=3), and the black horizontal lines represent the median value of all inputs grouped across replicates. Black lines connect measurements of CTB(+) and CTB(-) populations from the same biological replicate. Statistical significance was determined using a linear mixed model ANOVA with a post-hoc Bonferroni correction, followed by Benjamini-Hochberg FDR correction (α = 0.05) for multiple comparisons at each age/genotype. Black asterisks indicate significant eye-specific differences at each age. *p(adj)<0.05. (C) Eye-specific VGluT2 signal volume for all inputs separated by number of AZs in WT (left panel) and β2KO mice (right panel) at P4. (D) Average VGluT2 volume per AZ for all inputs separated by number of AZs in WT (left panel) and β2KO mice (right panel) at P4. In panels (C) and (D), error bars indicate group means ± SEMs (N=3 biological replicates for each age and genotype). Black dots represent mean values from separate biological replicates and black lines connect eye-specific measurements within each replicate. Statistical significance between eye-specific measurements was assessed for each genotype using two-tailed paired T-tests with Benjamini-Hochberg FDR correction (α = 0.05): *p(adj)<0.05.

clusters (separate AZs) in the first postnatal week. In WT mice, CTB(+) dominant-eye mAZ inputs contained more AZs than CTB(-) non-dominant-eye mAZ inputs at P4 and P8 (Fig. S2D). This maturation was delayed until P8 in β2KO mice (Fig. S2E). For CTB(+) dominant-eye inputs in both genotypes at P4, vesicle pool volume correlated positively with AZ number (**Fig. 3C**; Pearson correlation coefficients: WT [0.99] and β2KO [0.95]). A similar, but weaker correlation was observed for CTB(-) non-dominant-eye inputs (Pearson correlation coefficients: WT [0.97] and β2KO [0.90]. Dividing the total presynaptic VGluT2 volume by the AZ number revealed a consistent vesicle volume per AZ for both sAZ and mAZ inputs (**Fig. 3D**/S3, Table S3). Collectively, these results indicate that presynaptic vesicle pool volume scales with AZ number for each eye-specific input, while a dominant-eye bias persists throughout development.

Synapse clustering before eye-opening

Eye-specific competition is thought to involve stabilization of co-active, neighboring inputs from the same eye and elimination of out of sync inputs from the opposite eye [42–44]. Because axon refinement depends on the relative strength of neurotransmission between competing inputs [39, 45–51], mAZ inputs with multiple release sites could help stabilize nearby like-eye inputs [48, 52–54].

To quantify synaptic clustering patterns, we measured the distance from every eye-specific sAZ synapse to all other sAZ and mAZ inputs within each image field. sAZ synapses were often found nearby other inputs from the same eye (**Fig. 4A**). To define clustering, we searched volumetrically around each mAZ input and measured the fraction of sAZ synapses that were nearby at increasing distances (Fig. S4A/B). We then compared the observed percentages with datasets in which sAZ synapse positions were randomly shuffled within each neuropil volume. The largest differences occurred within a 1-2 μm search distance (Fig. S4A/B), and so we chose a 1.5 μm cutoff from the edge of each mAZ input to designate it “clustered” if at least one neighboring sAZ synapse lay within this distance and “isolated” if none did (**Fig. 4B**). No significant clustering was detected when sAZ and mAZ inputs originated from opposite eyes (Fig. S4C/D).

At the peak of competition in WT mice (P4), more than 65% of both mAZ and sAZ inputs were clustered for both eyes, while this proportion fell to ~50% in β2KO mice (**Fig. 4B**). In the WT dominant-eye projection, the fractions of clustered mAZ and sAZ inputs were similar at each age (**Fig. 4C**, top left panel). For the non-dominant eye projection, however, there were slightly more clustered mAZ inputs compared to clustered sAZ inputs at P4 (**Fig. 4C**, bottom left panel), the age when this eye adds sAZ synapses (**Fig. 2C**). β2KO mice showed no difference between mAZ and sAZ clustering at any age (**Fig. 4C**, right panels). Additionally, in WT mice at P4 and P8, clustered mAZ inputs from both eyes had marginally more neighboring sAZ synapses than did clustered sAZ synapses (**Fig. 4D**, left); this enrichment was absent in β2KO mice (**Fig. 4D**, right). Thus, while most retinogeniculate synapses lie within 1.5 μm of another like-eye input, WT mice show a tendency toward forming more synapses near mAZ inputs during synaptic competition.

Clustered mAZ inputs in P4 WT mice were also closer together than isolated mAZ inputs. Clustered mAZ inputs formed by the dominant-eye were ~32% closer to the nearest like-eye clustered mAZ input compared to isolated mAZ inputs (**Fig. 5A**, left panel). In the non-dominant eye projection, clustered mAZ inputs were ~55% closer together compared to isolated mAZ inputs (**Fig. 5B**, left panel). Once segregation was complete at P8, distances between clustered and isolated mAZ inputs were more similar (Fig. S5). In β2KO mice, distances between isolated and clustered mAZ inputs and their nearest clustered mAZ neighbor did not differ for either eye at P4 or P8 (**Fig. 5**/S5, right panels). These patterns are consistent with sAZ synapse addition when mAZ inputs are in close proximity during competition.

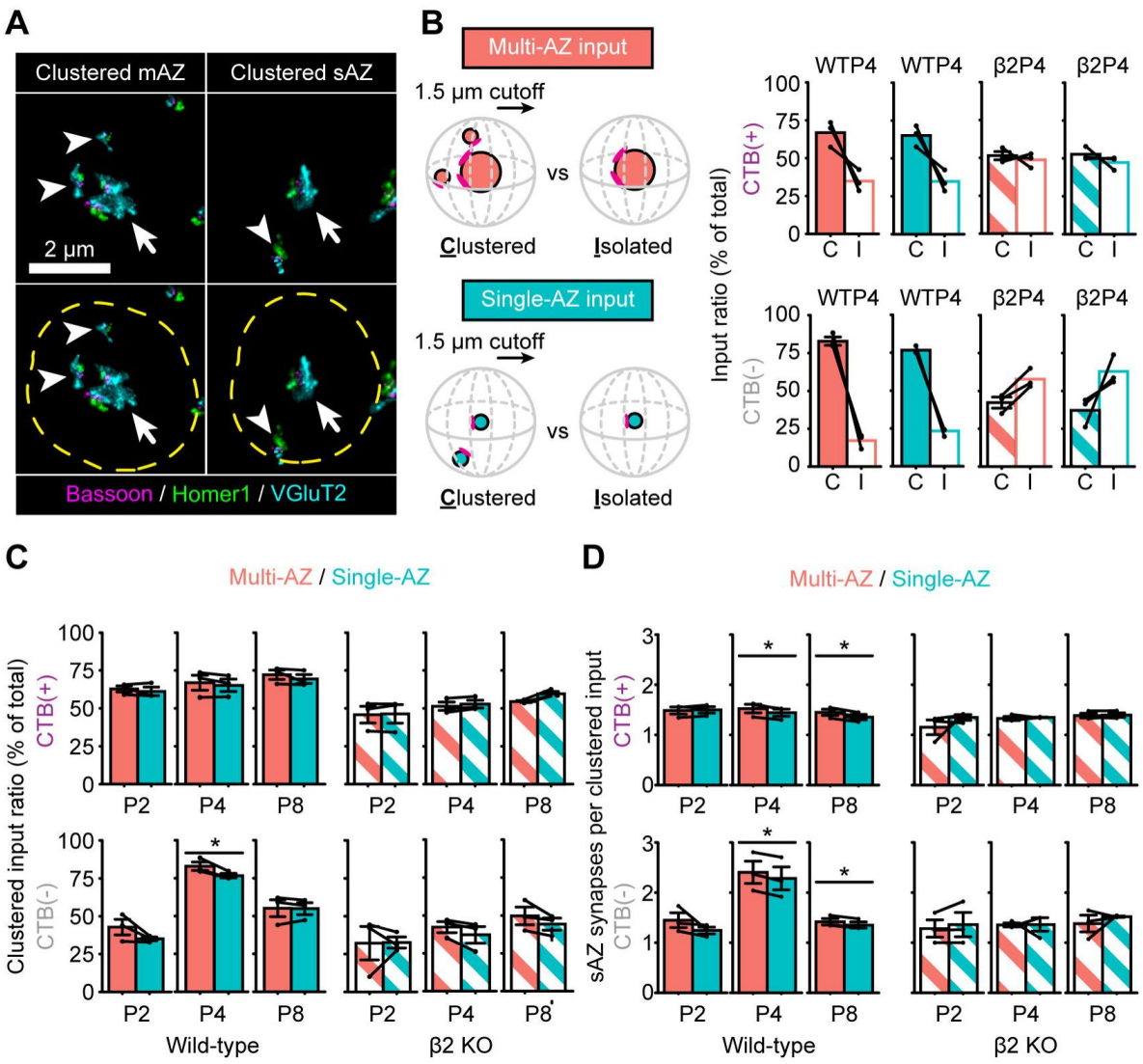

Fig. 4

Eye-specific synapse clustering before eye-opening

(A) Representative mAZ (left panels) and sAZ (right panels) inputs in a WT P8 sample with nearby sAZ synapses (arrowheads) clustered within 1.5 µm (dashed yellow ring). Arrows point to the centered mAZ or sAZ inputs. (B) Ratio of clustered and isolated mAZ and sAZ inputs for CTB(+) (upper panels) and CTB(-) (lower panels) inputs in WT and β2KO mice at P4. (C) Comparison of the clustered input ratio between mAZ and sAZ inputs across different ages, genotypes, and eyes of origin. (D) Comparison of the average number of nearby sAZ synapses for clustered mAZ and sAZ inputs across different ages, genotypes, and eyes of origin. In panels B-D, black dots represent mean values from separate biological replicates and black lines connect measurements within each replicate (N=3 for each age and genotype). Error bars represent group means ± SEMs. For each genotype, two-tailed paired T-tests with Benjamini-Hochberg FDR correction (α = 0.05) were used to test statistical significance between mAZ and sAZ inputs at each age. *p(adj)<0.05.

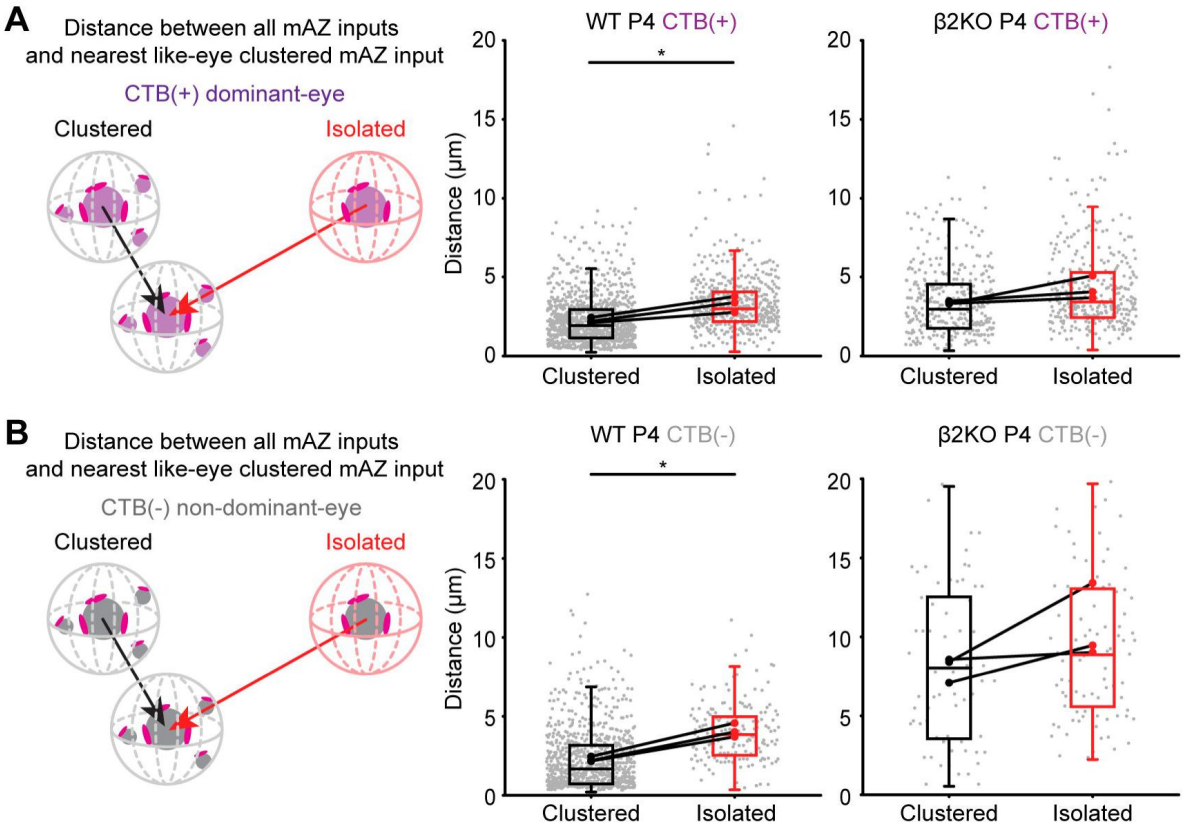

Fig. 5

Clustered mAZ inputs are closer than isolated inputs during competition

(A-B) Distance between clustered and isolated mAZ inputs and the closest like-eye clustered mAZ input, shown for (A) CTB(+) and (B) CTB(-) projections at P4 in WT and β2KO mice. Boxes indicate the 25%-75% distribution of input measurements from N=3 biological replicates and whiskers extend to 1.5 times the interquartile range. Gray dots represent individual distance measurements for all mAZ inputs. Black and red dots represent mean values from separate biological replicates and black lines connect measurements within each replicate (N=3 for each age and genotype). Statistical significance was determined using a linear mixed model ANOVA with post-hoc Bonferroni correction. For each genotype, p-values were corrected for multiple testing with Benjamini-Hochberg FDR correction (α = 0.05) at each age. Black asterisks indicate significant differences. *p(adj)<0.05.

Finally, we tested whether sAZ vesicle pool volume varies with distance to mAZ inputs. We classified each sAZ as "near" (≤1.5 μm) or "far" (>1.5 μm) relative to the nearest like-eye mAZ input. Across ages and genotypes, vesicle pool volume was similar for near and far sAZ synapses in both eyes (Fig. S6). Thus, vesicle pool size in sAZ synapses appears independent of their proximity to mAZ inputs.

Discussion

Spontaneous retinal activity guides eye-specific refinement by strengthening dominant eye inputs in the correct territory and pruning weaker inputs from the competing eye. Using volumetric super-resolution microscopy and eye-specific synaptic immunolabeling, we previously identified activity-dependent, eye-specific differences in presynaptic vesicle pool size and vesicle association with the active zone (AZ), both favoring the dominant eye during synaptic competition [26]. Here, we reanalyzed this dataset to measure synaptic spatial arrangements during normal development and how these are affected in a mutant model with abnormal eye-specific segregation.

Early input maturation and addition of release sites

Before eye-opening, retinal ganglion cell (RGC) axons from both eyes formed terminals with either multiple active zones (mAZ inputs) or a single active zone (sAZ synapses). Electron microscopy of dAPEX2-labeled ipsilateral RGC inputs revealed individual boutons with multiple active zones. Prior electron microscopy studies in mice showed no clustering from neighboring RGC boutons at postnatal day 8 [10, 11], suggesting the mAZ inputs seen in STORM images are single boutons containing multiple release sites. During competition, the dominant eye projection generated more of these mAZ inputs, each with more active zones and larger vesicle pools than the non-dominant eye. We observed a linear relationship between presynaptic vesicle signal volume and active zone number, suggesting that release site addition and vesicle pool expansion may be linked during input maturation. Functional recordings indicate that release site addition is the primary driver of retinogeniculate input strengthening after eye-opening [24]. Our findings reveal that eye-specific differences in release site addition at individual terminals emerge at the earliest stages of binocular refinement.

Spatial interactions during competition

Ipsilateral RGC axons are delayed in entering the dLGN until after contralateral inputs have already innervated the nucleus [55]. Despite their late arrival, these axons competed by forming numerous sAZ inputs, which equalized the overall input density between the eyes in the future contralateral eye domain at postnatal day 4 (P4). Most of these synapses formed nearby other like-eye neighbors, and were enriched near mAZ inputs, supporting the idea of release site addition at strong synapses. Neighboring sAZ synapses could ultimately mature into mAZ inputs as release sites are added and vesicle pools expand.

Distance analysis showed that clustered mAZ boutons were closer together than isolated mAZ boutons, further supporting release site addition near strong neighboring inputs. It remains unknown, however, whether nearby mAZ inputs originate from the same RGC. Nearby mAZ inputs within individual RGC arbors could promote release site addition via intrinsic mechanisms that scale with release site number, such as increased presynaptic calcium entry or surface delivery of synaptogenic molecules via presynaptic release. Boutons with multiple release sites could also trigger non-cell-autonomous signaling mechanisms that stabilize neighboring inputs from the same eye [48, 53, 54]. Release site addition increases extracellular glutamate concentration and promotes spillover onto adjacent synapses, which enhances the excitability of developing relay

cells [25] and could contribute to long term synaptic plasticity evoked by high frequency spiking in retinal wave bursts [56–59]. Consequently, release site addition and local bouton clustering may act in tandem to stabilize coactive inputs.

Competitive refinement also involves synapse elimination and axonal retraction through punishment signals. Genetic deletions of VGluT2 or RIM1 proteins in ipsilaterally-projecting RGCs decreased presynaptic vesicle release and prevented retraction of contralateral RGC axons from the ipsilateral territory [39, 45]. One downstream mediator of synaptic punishment is JAK2 kinase, which is phosphorylated in less active synapses [52]. Similar to neurotransmission mutant phenotypes, disruption of JAK2 signaling prevents axon retraction (punishment) during competition [52]. The spatial analyses we developed here will enable future mapping of input-specific punishment signals during synaptic competition. This includes phospho-JAK2 as well as molecular tags for glial pruning of weak inputs during eye-specific segregation [60–62].

Requirement for spontaneous retinal activity

β2KO mice showed significant defects in synapse addition during the first postnatal week. mAZs still formed with similar overall ratios as in wild type controls (Fig. S1, Table S3) and eye-specific differences in vesicle pool size still emerged. However, β2KO mice failed to form many sAZ synapses at the height of competition (P4), particularly in the late-arriving non-dominant (ipsilateral) eye projection. The failure to add synapses could explain the observation that synaptic clustering was reduced and more inputs formed in isolation in the mutants compared to controls.

While our results highlight developmental changes in presynaptic release site addition and clustering, activity-dependent postsynaptic mechanisms also influence input refinement at later stages. Retinogeniculate synapses undergo postsynaptic strengthening and weakening through potentiation and depression mediated by AMPARs and NMDARs [56–59]. After eye-specific segregation, spontaneous retinal activity is required for postsynaptic AMPAR insertion, synaptic strengthening, and elimination of weaker inputs [63]. Continued maintenance of segregation depends on calcium influx into relay neurons via L-type calcium channels, further implicating postsynaptic signaling in late-stage refinement [64, 65]. Input targeting may also be guided by molecular cues to form non-random, eye-specific connections with postsynaptic targets. Ipsilaterally-projecting RGCs have distinct gene expression profiles that specify axon guidance and may further support eye-specific synaptic targeting [66, 67]. Spontaneous retinal activity may permit axons to read out molecular regulators of synaptogenesis, as previously shown for RGC axon retraction [68].

Release site addition as a general mechanism underlying synaptic competition

Early synaptic clustering during retinogeniculate development resembles other circuits where neural activity guides competitive synaptic and axonal remodeling. At the neuromuscular junction (NMJ), motor neuron terminals compete for control of a postsynaptic muscle fiber; a single motor axon input strengthens while competing axons are eliminated [69–71]. Competition at the NMJ depends on inter-synaptic distance, with motor axons losing connections located near stronger competing synapses [69, 70]. As winning terminals are enlarged, presynaptic release site addition maintains a consistent density of Bassoon clusters (~2-3/μm^2) [72]. Neighboring inputs with weaker synaptic transmission are selectively eliminated [73, 74]. Competing motor axons differ in their release probabilities early in development [75], suggesting that presynaptic efficacy triggers local “stabilization” signals in winners and “punishment” signals in losers [76]. Presynaptic agrin release stabilizes postsynaptic receptor clusters by counteracting the destabilizing, dispersal effects of acetylcholine release, emphasizing the importance of early presynaptic transmission in postsynaptic stabilization [77, 78].

Similarly, in the developing cerebellum, Purkinje cells initially receive inputs from multiple climbing fibers (CFs) during the first postnatal week. Subsequently, one winning CF emerges and consolidates its synaptic inputs, while losing CFs are pruned [79, 80]. Here again, the winning input strengthens by adding presynaptic release sites, which increases multivesicular release and elevates glutamate concentration in the synaptic cleft [81–83]. Postsynaptic ultrastructural and molecular changes occur several days later as dominant CF inputs potentiate and losing CF inputs depress [82, 84, 85] through spike-timing dependent remodeling [86, 87]. Across these models, the earliest distinguishing feature between competing inputs is relative presynaptic transmission strength. Thus, release-site addition may be a conserved mechanism that biases synaptic refinement outcomes across developing neural circuits.

Materials and methods

The raw imaging data in this paper were previously reported [26]. Materials and methods below are adapted from this work. All Matlab and Python code used in the work is available on GitHub (*https://github.com/SpeerLab*). Raw STORM images of the full data are available on the open-access Brain Imaging Library [88]. These images can be accessed here: *https://doi.brainimagelibrary.org/doi/10.35077/g.1164*.

Animals

Wild-type C57BL/6J mice (Stock Number 000664) and APEX2 mice (Stock Number 032764) used in this study were purchased from the Jackson Laboratory. ET33^{Cre} mice and β2KO were generously gifted by Drs. Eric M. Ullian (University of California, San Francisco) and Michael C. Crair (Yale School of Medicine), respectively. All experimental procedures were performed in accordance with an animal study protocol approved by the Institutional Animal Care and Use Committee (IACUC) at the University of Maryland. Neonatal male and female mice were used interchangeably for all experiments. Tissue from biological replicates (N=3 animals) was collected for each age (P2/P4/P8) from each genotype (WT and β2KO) (18 animals total). Primers used for genotyping β2KO mice are: forward: CAGGCGTTATCCACAAAGACAGA; reverse: TTGAGGGGAGCAGAACAGAATC; mutant reverse: ACTTGGGTTTGGGCGTGTTGAG. Primers used for genotyping ET33Cre mice are: Forward: GGTCCTTGGCAGATGGGCAT; reverse: CGGCAAACGGACAGAAGCATT.

Electron microscopy tissue preparation

Animals were deeply anesthetized with ketamine/xylazine and transcardially perfused with 5-10 mls of 37°C 0.9% sterile saline (pH 7.2) followed by 20-30 mls of 37°C 4% EM-Grade paraformaldehyde (PFA, Electron Microscopy Sciences), 2% EM-Grade glutaraldehyde (GA, Electron Microscopy Sciences), 4mM calcium chloride ($CaCl_2$, Sigma-Aldrich) in 0.2M cacodylate buffer (pH 7.4). Brains were postfixed in the same perfusion fixative solution overnight at 4°C. Brains were vibratome sectioned in 0.2M cacodylate buffer (pH 7.4) at 100 µm. A circular tissue punch (~500 µm diameter) containing the dLGN was microdissected from each section using a blunt-end needle. dLGN sections were washed in 0.2M cacodylate buffer (pH 7.4) at 4°C on a rotator (4x 20 minutes each). Sections were incubated in 20mM glycine (Sigma-Aldrich) in 0.2M cacodylate buffer (pH 7.4) at 4°C on a rotator for 30 minutes, followed by 5 x 20 minutes washes in 0.2M cacodylate buffer (pH 7.4) at 4°C on a rotator. dLGN sections were immersed in 0.5mg/mL DAB solution, covered with foil, for 30 minutes at 4°C on a rotator. 10 µL of 0.03% hydrogen peroxide (Sigma-Aldrich) was mixed into the DAB solution (1 mL) and incubated for 10 minutes at 4°C on a rotator (light protected). The reaction was quenched with 0.2M cacodylate buffer (pH 7.4) washes (3 x 1-minute washes followed by 2 x 20 minutes washes).

Tissue preparation for scanning electron microscopy

dLGN sections were fixed in 2% osmium tetroxide (Electron Microscopy Sciences) in 0.15M cacodylate buffer (pH 7.4) for 45 minutes at room temperature. Sections were reduced with 2.5% potassium ferricyanide (Electron Microscopy Sciences) in 0.15M cacodylate buffer (pH 7.4) for 45 minutes at room temperature in the dark, followed by 2 x 10-minute washes in double distilled water. Sections were incubated in 1% aqueous thiocarbohydrazide (Electron Microscopy Sciences) for 20 minutes, followed by 2 x 10-minute washes in double distilled water. Samples were fixed in 1% aqueous osmium tetroxide for 45 minutes at room temperature, followed by 2 x 10-minute washes in double distilled water. Sections were postfixed in 1% uranyl acetate (Electron Microscopy Sciences) in 25% ethanol in the dark for 20 minutes at room temperature and washed and stored in double distilled water overnight. The next day, samples were stained with aqueous lead aspartate at 60°C for 30 minutes and washed with double distilled water 2 x 10 minutes. Tissues were dehydrated in a graded dilution series of 100% ethanol (35%; 50%; 70%; 95%; 100%; 100%; 100% EtOH) for 10 minutes each at room temperature. Samples were immersed in propylene oxide (Electron Microscopy Sciences) 3 x 10 minutes at room temperature, followed by a series of epon resin/propylene oxide (812 Epon Resin, Electron Microscopy Sciences) exchanges with increasing resin concentrations (50% resin/50% propylene oxide; 65% resin/35% propylene oxide; 75% resin/25% propylene oxide; 100% resin; 100% resin) for 90 minutes each. Tissues were transferred to BEEM capsules (Electron Microscopy Sciences) that were filled with 100% resin and polymerized for at least 48 hours at 60°C.

Transmission electron microscopy image acquisition

Plasticized sections were cut at 70 nm with a Histo Jumbo diamond knife (DiATOME) using a Leica UC7 ultramicrotome. Sections were decompressed using chloroform vapor and collected onto 3.05mm 200 mesh Gilder thin bar hexagonal mesh copper grids (T200H-Cu, Electron Microscopy Sciences). Sections were imaged unstained on a Hitachi HT7700 transmission electron microscope (HT7700, Hitachi High-Tech America, Inc.) at 80kV.

Eye injections

Intraocular eye injections were performed one day before tissue collection. Briefly, mice were anesthetized by inhalant isoflurane and sterile surgical spring scissors were used to gently part the eyelid to expose the corneoscleral junction. A small hole was made in the eye using a sterile 34-gauge needle and ~0.5 µL of cholera toxin subunit B conjugated with Alexa Fluor 488 (CTB-488, ThermoFisher Scientific, Catalogue Number: C34775) diluted in 0.9% sterile saline was intravitreally pressure-injected into the right eye using a pulled-glass micropipette coupled to a Picospritzer (Parker Hannifin).

dLGN tissue preparation for STORM imaging

Animals were deeply anesthetized with ketamine/xylazine and transcardially perfused with 5-10 mls of 37°C 0.9% sterile saline followed by 10 mls of room temperature 4% EM-Grade paraformaldehyde (PFA, Electron Microscopy Sciences) in 0.9% saline. Brains were embedded in 2.5% agarose and vibratome sectioned in the coronal plane at 100 µm. From the full anterior-posterior series of dLGN sections (~6-8 sections) we selected the central two sections for staining in all biological replicates. These sections were morphologically consistent with Figs. 134-136 (5.07-5.31 mm) of the postnatal day 6 mouse brain from Paxinos's "Atlas of the developing mouse brain" Academic Press, 2020 [89]. Selected sections were postfixed in 4% PFA for 30 minutes at room temperature and washed for 30-40 minutes in 1X PBS. The dLGN was identified by the presence of CTB-488 signals using a fluorescence dissecting microscope. A circular tissue punch (~500 µm diameter) containing the dLGN was microdissected from each section using a blunt-end needle. A small microknife cut was made at the dorsal edge of the dLGN which, together with the CTB-488 signal, enabled us to identify the dLGN orientation during image acquisition.

Immunohistochemistry

We used a serial-section single-molecule localization imaging approach to prepare samples and collect super-resolution fluorescence imaging volumes as previously described [26]. dLGN tissue punches were blocked in 10% normal donkey serum (Jackson ImmunoResearch, Catalogue Number: 017-000-121) with 0.3% Triton X-100 (Sigma-Aldrich Inc.) and 0.02% sodium azide (Sigma-Aldrich Inc.) diluted in 1X PBS for 2-3 hours at room temperature and then incubated in primary antibodies for ~72 hours at 4°C. Primary antibodies used were Rabbit anti-Homer1 (Synaptic Systems, Catalogue Number: 160003, 1:100) to label postsynaptic densities (PSDs), mouse anti-Bassoon (Abcam, Catalogue Number AB82958, 1:100) to label presynaptic active zones (AZs), and guinea pig anti-VGluT2 (Millipore, Catalogue Number AB251-I, 1:100) to label presynaptic vesicles. Following primary antibody incubation, tissues were washed in 1X PBS for 6 x 20 minutes at room temperature and incubated in secondary antibody solution overnight for ~36 hours at 4°C. The secondary antibodies used were donkey anti-rabbit IgG (Jackson ImmunoResearch, Catalogue Number 711-005-152, 1:100) conjugated with Dy749P1 (Dyomics, Catalogue Number 749P1-01) and Alexa Fluor 405 (ThermoFisher, Catalogue Number: A30000), donkey anti-mouse IgG (Jackson ImmunoResearch, Catalogue Number 715-005-150, 1:100) conjugated with Alexa Fluor 647 (ThermoFisher, Catalogue Number: A20006) and Alexa Fluor 405, and donkey anti-guinea pig IgG (Jackson ImmunoResearch, Catalogue Number 706-005-148, 1:100) conjugated with Cy3b (Cytiva, Catalogue Number: PA63101). Tissues were washed 6 x 20 minutes in 1X PBS at room temperature after secondary antibody incubation.

Postfixation, dehydration, and embedding in epoxy resin

Tissue embedding was performed as previously described [26]. Tissues were postfixed with 3% PFA + 0.1% GA (Electron Microscopy Sciences) in PBS for 2 hours at room temperature and then washed in 1X PBS for 20 minutes. To plasticize the tissues for ultrasectioning, the tissues were first dehydrated in a graded dilution series of 100% ethanol (50%/70%/90%/100%/100% EtOH) for 15 minutes each at room temperature and then immersed in a series of epoxy resin/100% EtOH exchanges (Electron Microscopy Sciences) with increasing resin concentration (25% resin/75% ethanol; 50% resin/50% ethanol; 75% resin/25% ethanol; 100% resin; 100% resin) for 2 hours each. Tissues were transferred to BEEM capsules (Electron Microscopy Sciences) that were filled with 100% resin and polymerized for 16 hours at 70°C.

Ultrasectioning

Plasticized tissue sections were cut using a Leica UC7 ultramicrotome at 70 nm using a Histo Jumbo diamond knife (DiATOME). Chloroform vapor was used to reduce compression after cutting. For each sample, ~100 sections were collected on a coverslip coated with 0.5% gelatin and 0.05% chromium potassium (Sigma-Aldrich Inc.), dried at 60 degrees for 25 minutes, and protected from light prior to imaging.

Imaging chamber preparation

Coverslips were chemically etched in 10% sodium ethoxide for 5 minutes at room temperature to remove the epoxy resin and expose the dyes to the imaging buffer for optimal photoswitching. Coverslips were then rinsed with ethanol and dH_2O. To create fiducial beads for flat-field and chromatic corrections, we mixed 715/755nm and 540/560nm, carboxylate-modified microspheres (Invitrogen, Catalogue Numbers F8799 and F8809, 1:8 ratio respectively) to create a high-density fiducial marker and then further diluted the mixture at 1:750 with Dulbecco's PBS to create a low-density bead solution. Both high- and low-density bead solutions were spotted on the coverslip (~0.7 µL each) for flat-field and chromatic aberration correction respectively. Excess beads were rinsed away with dH2O for 1-2 minutes. The coverslip was attached to a glass slide with double-

sided tape to form an imaging chamber. The chamber was filled with STORM imaging buffer (10% glucose, 17.5μM glucose oxidase, 708nM catalase, 10mM MEA, 10mM NaCl, and 200mM Tris) and sealed with epoxy.

Imaging setup

Imaging was performed using a custom single-molecule super-resolution imaging system. The microscope contained low (4x/10x air) and high (60x 1.4NA oil immersion) magnitude objectives mounted on a commercial frame (Nikon Ti-U) with back optics arranged for oblique incident angle illumination. We used continuous-wave lasers at 488nm (Coherent), 561nm (MPB), 647nm (MPB), and 750nm (MPB) to excite Alexa 488, Cy3B, Alexa 647, and Dy749P1 dyes respectively. A 405 nm cube laser (Coherent) was used to reactivate Dy749P1 and Alexa647 dye photoswitching. The microscope was fitted with a custom pentaband/pentanotch dichroic filter set and a motorized emission filter wheel. The microscope also contained an IR laser-based focus lock system to maintain optimal focus during automatic image acquisition. Images were collected on 640*640-pixel region of an sCMOS camera (ORCA-Flash4.0 V3, Hamamatsu Photonics) with a pixel size of ~155 nm.

Automated image acquisition

Fiducials and tissue sections on the coverslip were imaged using the low magnification objective (4X) to create a mosaic overview of the specimen. Beads/sections were then imaged at high magnification (60X) to select regions of interest (ROIs) in the Cy3B and Alexa 488 channels. Before final image acquisition, laser intensities and the incident angle were adjusted to optimize photoswitching for STORM imaging and utilize the full dynamic range of the camera for conventional imaging.

Low-density bead images were taken in 16 partially overlapping ROIs. 715/755nm beads were excited using 750 nm light and images were collected through Dy749P1 and Alexa 647 emission filters. 540/560nm beads were excited using a 488 nm laser and images were collected through Alexa 647, Cy3B, and Alexa 488 emission filters. These fiducial images were later used to generate a non-linear warping transform to correct chromatic aberration. Next, ROIs within each tissue section were imaged at conventional (diffraction-limited) resolution in all four-color channels sequentially.

Following conventional image acquisition, a partially overlapping series of 9 images were collected in the high-density bead field for all 4 channels (Dy749P1, Alexa 647, Cy3B, and Alexa 488). These images were later used to perform a flat-field image correction of non-uniform laser illumination across the ROIs. Another round of bead images was taken as described above in a different ROI of the low-density bead field. These images were later used to confirm the stability of chromatic offsets during imaging. All ROIs within physical sections were then imaged by STORM for Dy749P1 and Alexa 647 channels. Images were acquired using a custom progression of increasing 405nm laser intensity to control single-molecule switching. 8000 frames of Dy749P1 channel images were collected (60 Hz imaging) followed by 12000 frames of Alexa 647 channel images (100 Hz). In a second imaging pass, the same ROIs were imaged for Cy3B and Alexa 488 channels, each for 8000 frames (60 Hz).

We imaged the ipsilateral and contralateral ROIs separately in each physical section of the dLGN. For consistency of ROI selection across biological replicates at each age, we identified the dorsal-ventral (DV) axis of the dLGN and selected ROIs within the center (core region) at 2/5 (ipsilateral ROI) and 4/5 (contralateral ROI) of the full DV length

Image processing

Single-molecule localization was performed using a previously described DAOSTORM algorithm modified for use with sCMOS cameras [90], [91]. Molecule lists were rendered as 8-bit images with 15.5 nm pixel size where each molecule is plotted as an intensity distribution with an area reflecting its localization precision. Low-density fiducial images were used for chromatic aberration correction. We localized 715/755 beads in Dy749P1 and Alexa 647 channels, and 540/560 beads in Alexa 647, Cy3B, and Alexa 488 channels. A third-order polynomial transform map was generated by matching the positions of each bead in all channels to the Alexa 647 channel. The average residual error of bead matching was <15 nm for all channels. The transform maps were applied to both 4-color conventional and STORM images. Conventional images were upscaled (by 10X) to match the STORM image size. The method to align serial sections was previously described [26]. STORM images were first aligned to their corresponding conventional images by image correlation. To generate an aligned 3D image stack from serial sections, we normalized the intensity of all Alexa 488 images and used these normalized images to generate both rigid and elastic transformation matrices for all four-color channels of both STORM and conventional data. The final image stack was then rotated and cropped to exclude incompletely imaged edge areas. To further confirm that the processed region corresponds to the contralateral dLGN, conventional CTB(+) signals of the labeled contralateral projection were thresholded to create a polygonal mask (a convex hull analysis linking the outermost CTB signals in the image volume). The mask was then applied to STORM images to exclude peripheral areas where CTB signals were absent or faint.

Cell body filter

The aligned STORM images had non-specific labeling of cell bodies in Dy749P1 and Alexa 647 channels corresponding to Homer1 and Bassoon immunolabels. To limit synaptic cluster identification to the neuropil region we identified cell bodies based on their Dy749P1 signal and excluded these regions from further image processing. STORM images were convolved with a Gaussian function (σ=140 nm) and then binarized using the lower threshold of a two-level Otsu threshold method. We located connected components in the thresholded images and generated a mask based on components larger than e[11] voxels. Because cell body clusters were orders of magnitude larger than synaptic clusters, the cell body filter algorithm was robust to a range of size thresholds. The mask was applied to images of all channels to exclude cell body areas.

Eye-specific synapse identification and quantification

To correct for minor variance in image intensity across physical sections, we normalized the pixel intensity histogram of each section to the average histogram of all sections. Image histograms were rescaled to make full use of the 8-bit range. Using a two-level Otsu threshold method, the conventional images were thresholded into three classes: a low-intensity background, low-intensity signals above the background representing non-synaptic labeling, and high-intensity signals representing synaptic structures. The conventional images were binarized by the lower two-level Otsu threshold, generating a mask for STORM images to filter out background signals. STORM images were convolved with a Gaussian function (σ= 77.5 nm) and thresholded using the higher two-level Otsu threshold. Following thresholding, connected components were identified in three dimensions using MATLAB ‘conncomp’ function. A watershedding approach was applied to split large clusters that were improperly connected. Clusters were kept for further analysis only if they contained aligned image information across two or more physical sections. We also removed all edge synapses from our analysis by excluding synapses that did not have blank image data on all adjacent sides.

To distinguish non-specific immunolabeling from true synaptic signals, we quantified two parameters for each cluster: cluster volume and cluster signal density calculated by the ratio of within-cluster pixels with positive signal intensity in the raw STORM images. Two separate populations were identified in 2D histograms plotted from these two parameters. We manually selected the population with higher volumes and signal densities representing synaptic structures. To test the robustness of the manual selection, we performed multiple repeated measurements of the same data and discovered a between-measurement variance of <1% (data not shown).

To identify paired pre- and postsynaptic clusters, we first measured the centroid-centroid distance of each cluster in the Dy749P1 (Homer1) and Alexa 647 (Bassoon) channels to the closest cluster in the other channel. We next quantified the signal intensity of each opposing synaptic channel within a 140 nm shell surrounding each cluster. A 2D histogram was plotted based on the measured centroid-centroid distances and opposing channel signal densities of each cluster. Paired clusters with closely positioned centroids and high intensities of apposed channel signal were identified using the OPTICS algorithm. Retinogeniculate synapses were identified by pairing Bassoon (Alexa 647) clusters with VGluT2 (Cy3B) clusters using the same method as pre/post-synaptic pairing. Synapses from the right eye were identified by pairing VGluT2 clusters with CTB (Alexa 488) clusters. The volume of each cluster reflected the total voxel volume of all connected voxels, and the total signal intensity was a sum of voxel intensity within the volume of the connected voxels.

Multi-AZ synapse identification and quantification

To determine whether an eye-specific VGluT2 cluster is a mAZ synapse or a sAZ synapse, we measured the number of active zones (defined by individual Bassoon clusters) associated with each VGluT2 cluster in the dataset. A 3D shell was extended 140 nm from the surface voxels of each VGluT2 cluster and any Bassoon clusters that fell within the shell were considered to be associated with the target VGluT2 cluster. The number of active zones (AZs) associated with each VGluT2 cluster was then measured. VGluT2 clusters associated with more than 1 AZ were defined as mAZ synapses, while those associated with only 1 AZ were defined as sAZ synapses.

Quantification of mAZ and sAZ synapse VGluT2 cluster volume was performed using the “regionprops” function in MATLAB, which provided the voxel size and weighted centroid of each VGluT2 cluster. The search for sAZ synapses adjacent to mAZ synapses (synaptic clustering analysis) was conducted using a similar search approach as for associated Bassoon clusters, with expansion shell sizes ranging from 1 μm to 4 μm from the surface voxels of each mAZ synapse. The main Figs. in the study utilized an expansion distance of 1.5 μm. An eye-specific sAZ synapse was considered to be near a mAZ synapse if its weighted centroid fell within the expanded volume.

Quantification and statistical analysis

Statistical analysis was performed using SPSS. Plots were generated by SPSS or R (ggplot2). Statistical details are presented in the figure legends and supplemental tables S2/S3. For all measurements in this paper, we analyzed N = 3 biological replicates (individual mice) for each genotype (WT and β2KO) at each age (P2, P4, and P8). Cluster densities, synapse AZ number, average VGluT2 cluster volume, and all fractional measurements were presented as mean ± SEM values in paired bar graphs and statistical analysis was performed using two-tailed paired T-tests. Nonparametric Kolmogorov-Smirnov tests were used in all cumulative histogram comparisons. We used a linear mixed model to compare VGluT2 cluster volumes (**Figs. 3** and S2) and distance measurements (**Figs. 5** and S5). For VGluT2 cluster volume comparisons, the age or eye-of-origin was the fixed main factor and biological replicate IDs were nested random factors. In distance measurement comparisons, the mAZ synapse AZ number was the fixed main factor and biological replicate IDs were nested random factors. Effect sizes were calculated using Cohen’s d for parametric tests and epsilon squared for nonparametric tests. To address multiple testing, we applied false discovery rate (FDR) correction using the Benjamini-Hochberg method with $\alpha = 0.05$

separately within each experimental condition (P2-WT, P2-ß2KO, P4-WT, P4-ß2KO, P8-WT, P8-ß2KO). 20-34 measurements (varying by age and genotype) were corrected within each of the six experimental conditions, resulting in condition-specific FDR-adjusted p-values presented in Table S2. In violin plots, each violin showed the distribution of grouped data from all biological replicates from the same condition. Each black dot represents the median value of each biological replicate, and the horizontal black line represents the group median. Black lines connect measurements of CTB(+) and CTB(-) populations from the same biological replicate. Asterisks in all figures indicate statistical significance after FDR correction: *p(adj)<0.05. For VGluT2 volume comparisons, we calculated 5/95% confidence intervals based on the linear mixed model. 5/95% confidence intervals in synapse densities, AZ numbers, and distances were calculated for paired or unpaired data comparisons using SPSS. All statistical results are listed in Table S2. All conclusions we draw in the main text from the data have corresponding confidence intervals listed in both the figure legends and Table S3.

Data availability

All Matlab and Python code used in the work is available on GitHub (*https://github.com/SpeerLab*). Raw STORM images of the full data are available on the open-access Brain Imaging Library: *https://doi.brainimagelibrary.org/doi/10.35077/g.1164*.

Acknowledgements

We thank Drs. Michael C. Crair (Yale University) and Eric M. Ullian (University of California, San Francisco) for generously sharing the β2KO and ET33^{Cre} mouse lines used in this work. We are grateful to Tim Maugel in the Laboratory for Biological Ultrastructure (UMD) for his assistance with transmission electron microscopy experiments. The research was funded by National Institutes of Health grant DP2MH125812 (C.M.S.).

Additional information

Author contributions

Conceptualization, C.Z. and C.M.S.; data curation, C.Z., T.V., C.M.S.; formal analysis, C.Z. and C.M.S.; funding acquisition, C.M.S.; investigation, C.Z., T.V., C.M.S.; methodology, C.Z., T.V., C.M.S.; project administration, C.Z. and C.M.S.; resources, C.Z., T.V., C.M.S.; software, C.Z. and C.M.S.; supervision, C.M.S.; validation, C.Z., T.V., C.M.S.; visualization, C.Z., T.V., C.M.S.; writing – original draft preparation, C.Z. and C.M.S.; writing – review & editing, C.Z., T.V., C.M.S.

Funding

HHS | National Institutes of Health (NIH) (DP2MH125812)

- Tarlan Vatan
- Chenghang Zhang

Additional files

Supplemental Table S1

Supplemental Table S2

Supplemental Table S3

Supplementary figures

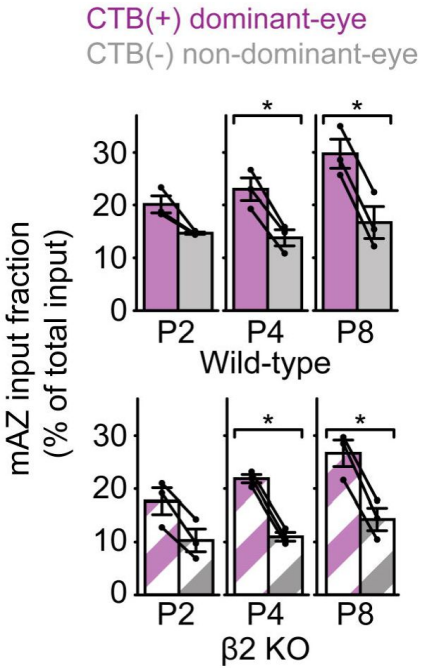

Fig. S1

Fraction of mAZ inputs across development, related to

Fig. 2 Eye-specific mAZ input fraction across development in WT (top panel) and β2KO mice (bottom panel). Black dots represent mean values from separate biological replicates and black lines connect measurements within each replicate (N=3 for each age and genotype). Error bars represent group means ± SEMs. Statistical significance between eye-specific measurements was assessed for each genotype using two-tailed paired T-tests with Benjamini-Hochberg FDR correction (α = 0.05) at each age. *p(adj)<0.05.

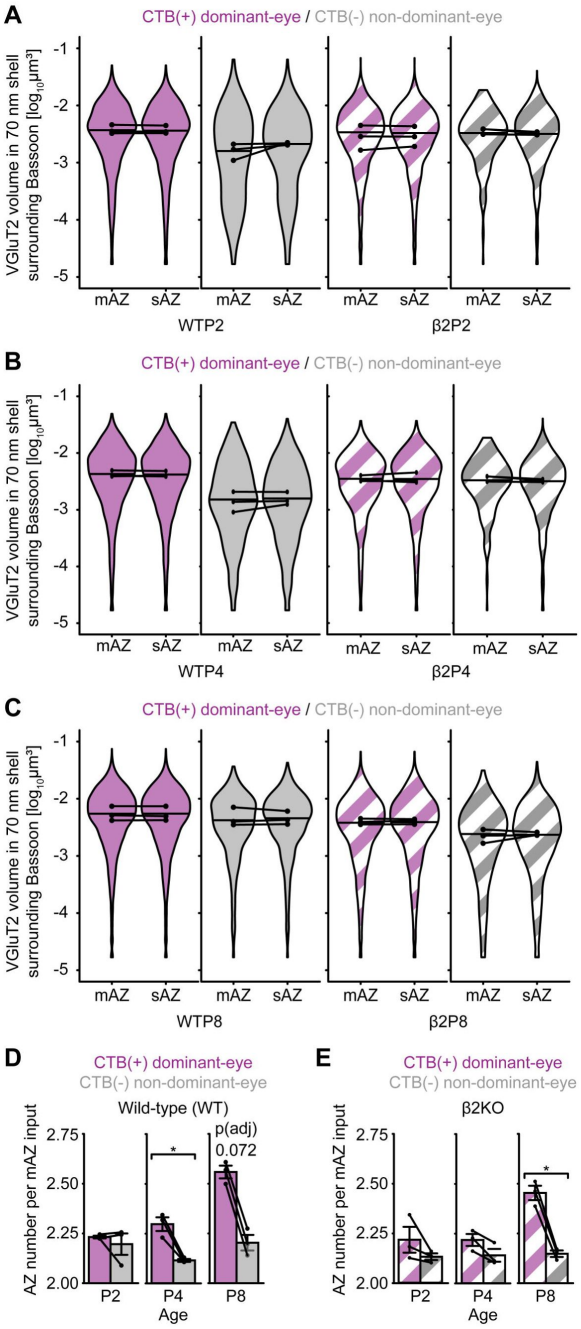

Fig. S2

Quantification of docked vesicle pool volume and AZ number in mAZ and sAZ inputs, related to

Fig. 2. (A-C) Violin plots show the distribution of VGluT2 cluster volume within a 70 nm shell surround individual Bassoon clusters at (A) P2, (B) P4, and (C) P8. The width of each violin plot reflects the relative synapse proportions at each volume across the entire grouped data set (N=3 biological replicates). The maximum width of the violin plots was normalized across all groups. Black horizontal lines represent the median value of all inputs grouped across replicates. The black dots represent the median value of each biological replicate and black lines between dots connect measurements from the same biological replicate. Statistical significance was determined using a linear mixed model ANOVA with post-hoc Bonferroni correction. See Table S3 for 5/95% confidence intervals. (D-E) Average AZ number per mAZ input in (D) WT and (E) β2KO mice. Black dots represent mean values from separate biological replicates (N = 3) and black lines connect measurements within each replicate. Error bars represent means ± SEMs. Statistical significance was assessed for each genotype using two-tailed paired T-tests with Benjamini-Hochberg FDR correction (α = 0.05) at each age. *p(adj)<0.05.

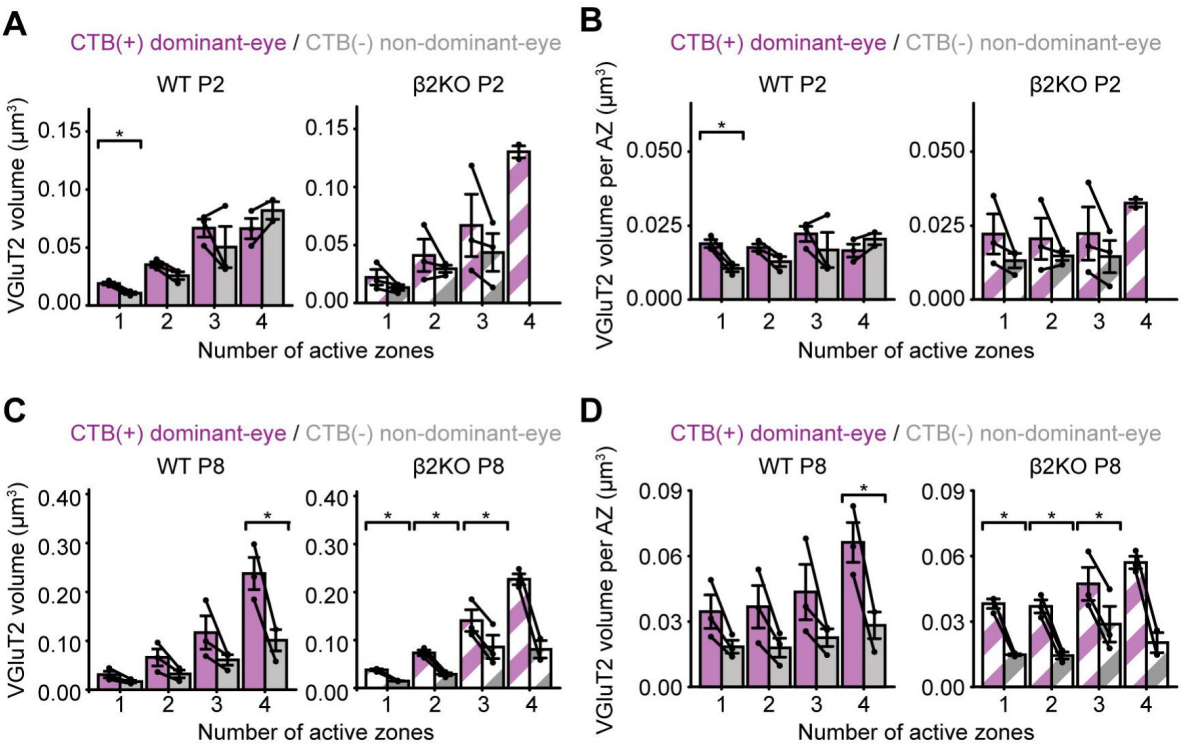

Fig. S3

Relationship between vesicle pool volume and active zone number, related to

Fig. 3. (A) Total VGluT2 volume per input and (B) average VGluT2 volume per AZ for all inputs separated by number of AZs in WT (filled bars) and β2KO mice (striped bars) at P2. (C) Total VGluT2 volume per input and (D) average VGluT2 volume per AZ for all inputs separated by number of AZs in WT (filled bars) and β2KO mice (striped bars) at P8. In all panels, error bars indicate group means ± SEMs (N=3 biological replicates for each age and genotype). Black dots represent mean values from separate biological replicates and black lines connect measurements within each replicate. Statistical significance between eye-specific measurements was assessed for each genotype using two-tailed paired T-tests with Benjamini-Hochberg FDR correction (α = 0.05) at each age: *p(adj)<0.05.

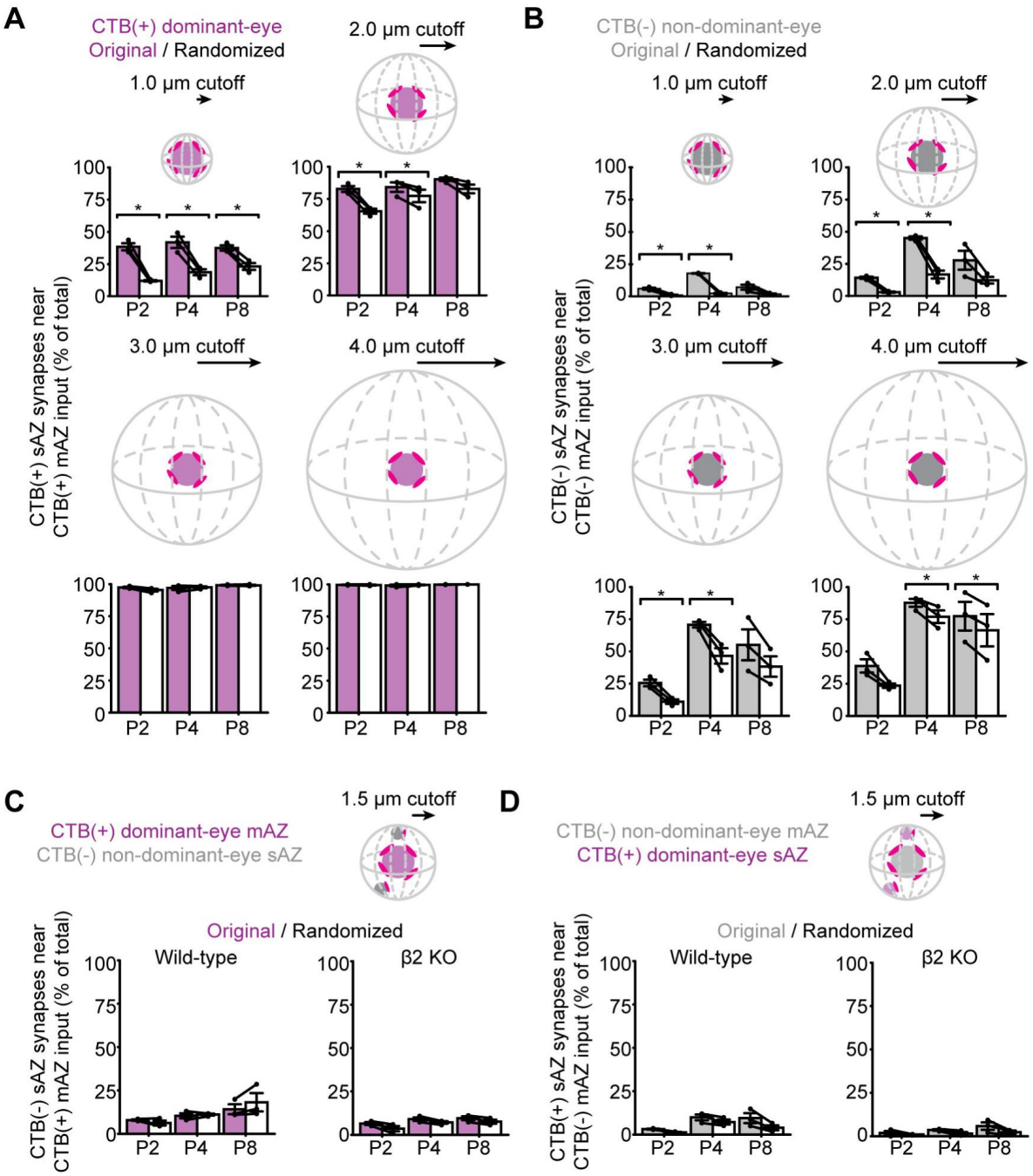

Fig. S4

sAZ synapse clustering near like-eye mAZ inputs, related to

Fig. 4 (A) The ratio of CTB(+) dominant-eye and (B) CTB(-) non-dominant-eye sAZ synapses nearby like-eye mAZ inputs within increasing distance cutoffs in WT samples across ages. At distances of 1-2 µm across all ages, the observed ratios (filled bars) are higher than a reshuffling of the data (open bars) where the position of sAZ inputs was randomized within the neuropil. (C-D) Percentage of sAZ synapses within 1.5 µm of opposite-eye mAZ inputs across ages in WT and β2KO mice. Data are compared against a randomization of sAZ positions (open bars) as in panels A/B. For all panels, error bars represent group means ± SEMs (N=3 biological replicates for each age and genotype). Black dots represent mean values from separate biological replicates and black lines connect measurements within each replicate. Statistical significance was assessed for each genotype using two-tailed paired T-tests with Benjamini-Hochberg FDR correction (α = 0.05) at each age: *p(adj)<0.05.

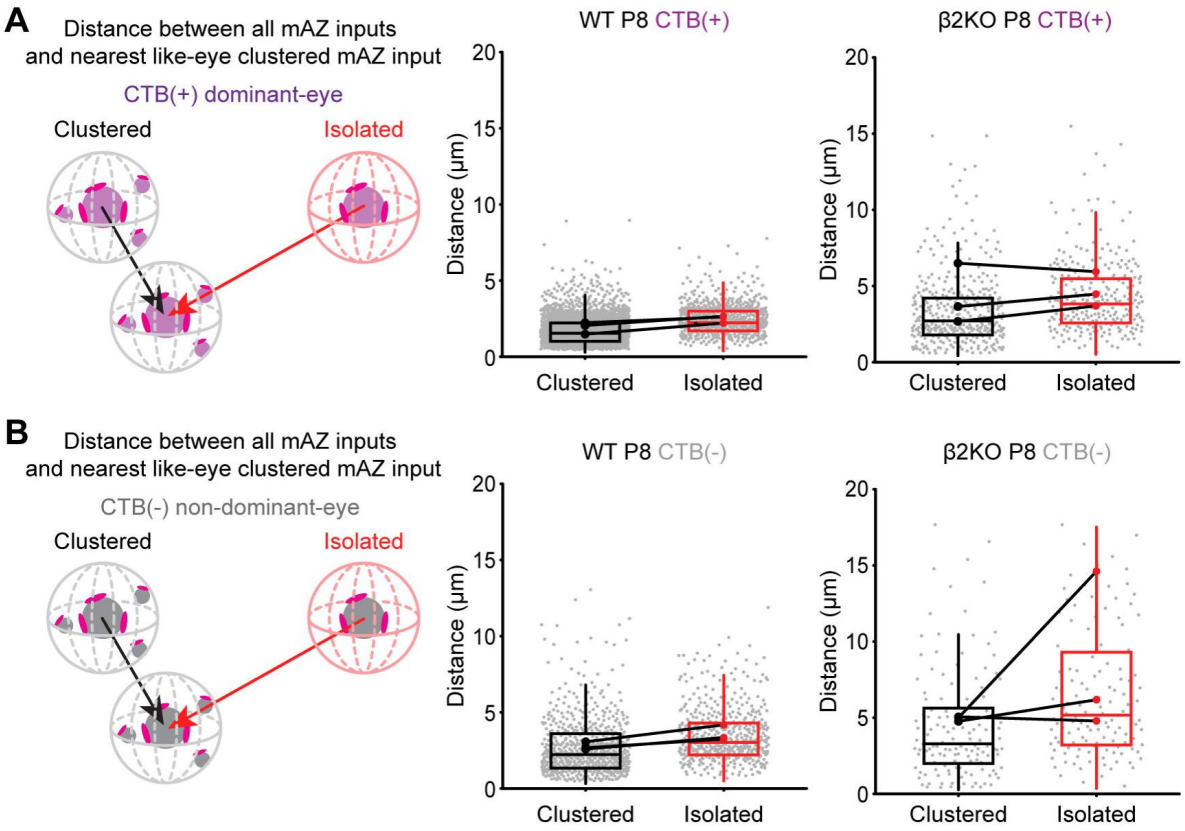

Fig. S5

Clustered and isolated mAZ inputs show similar spacing after competition, related to

Fig. 5. (A-B) Distance between clustered and isolated mAZ inputs and the closest like-eye clustered mAZ input, shown for (A) CTB(+) and (B) CTB(-) projections at P8 in WT and β2KO mice. Boxes indicate the 25%-75% distribution of input measurements from N=3 biological replicates and whiskers extend to 1.5 times the interquartile range. Gray dots represent individual distance measurements for all mAZ inputs. Black and red dots represent mean values from separate biological replicates and black lines connect measurements within each replicate (N=3 for each age and genotype). Statistical significance was determined using a linear mixed model ANOVA with post-hoc Bonferroni correction (see Table S3 for 5/95% confidence intervals). For each genotype, p-values were corrected for multiple testing with Benjamini-Hochberg FDR correction (α = 0.05) at each age.

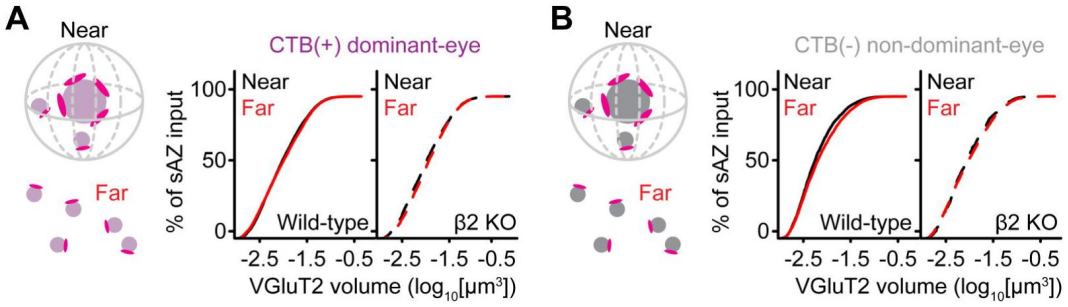

Fig. S6

sAZ synapse vesicle pool volume is independent of distance to mAZ inputs, related to

Fig. 5. (A) Cumulative distributions of VGluT2 volume for CTB(+) dominant-eye or (B) CTB(-) non-dominant-eye sAZ synapses near (<1.5 μm) or far from (>1.5 μm) like-eye mAZ inputs. The distributions show merged data across all ages (P2/P4/P8; N=3 biological replicates at each time point). A nonparametric Kolmogorov-Smirnov test was used for statistical analysis (see Table S3 for 5/95% confidence intervals). For each genotype, p-values were corrected for multiple testing with Benjamini-Hochberg FDR correction (α = 0.05) at each age.

References

1. Rall W (1962) **Electrophysiology of a dendritic neuron model** *Biophys J* **2**:145–67 https://doi.org/10.1016/s0006-3495(62)86953-7 | PubMed | Google Scholar

2. Mel B (1991) **The Clusteron: Toward a Simple Abstraction for a Complex Neuron** Morgan-Kaufmann Google Scholar

3. Poirazi P, Mel BW (2001) **Impact of active dendrites and structural plasticity on the memory capacity of neural tissue** *Neuron* **29**:779–96 https://doi.org/10.1016/s0896-6273(01)00252-5 | PubMed | Google Scholar

4. Mel BW, Schiller J, Poirazi P (2017) **Synaptic plasticity in dendrites: complications and coping strategies** *Curr Opin Neurobiol* **43**:177–86 https://doi.org/10.1016/j.conb.2017.03.012 | PubMed | Google Scholar

5. Kastellakis G, Poirazi P (2019) **Synaptic Clustering and Memory Formation** *Front Mol Neurosci* **12**:300 https://doi.org/10.3389/fnmol.2019.00300 | PubMed | Google Scholar

6. Winnubst J, Lohmann C (2012) **Synaptic clustering during development and learning: the why, when, and how** *Front Mol Neurosci* **5** https://doi.org/10.3389/fnmol.2012.00070 | PubMed | Google Scholar

7. Leighton AH, Lohmann C (2016) **The Wiring of Developing Sensory Circuits-From Patterned Spontaneous Activity to Synaptic Plasticity Mechanisms** *Front Neural Circuits* **10** https://doi.org/10.3389/fncir.2016.00071 | PubMed | Google Scholar

8. Kirchner JH, Gjorgjieva J (2022) **Emergence of synaptic organization and computation in dendrites** *Neuroforum* **28**:21–30 https://doi.org/10.1515/nf-2021-0031 | Google Scholar

9. Liang L, Chen C., Organization (2020) **Function, and Development of the Mouse Retinogeniculate Synapse** *Annu Rev Vis Sci* **6**:261–85 https://doi.org/10.1146/annurev-vision-121219-081753 | PubMed | Google Scholar

10. Bickford ME, Slusarczyk A, Dilger EK, Krahe TE, Kucuk C, Guido W (2010) **Synaptic development of the mouse dorsal lateral geniculate nucleus** *J Comp Neurol* **518**:622–35 https://doi.org/10.1002/cne.22223 | PubMed | Google Scholar

11. Monavarfeshani A, Stanton G, Van Name J, Su K, Mills WA, Swilling K, Kerr A, Huebschman NA, Su J (2018) **Fox MA. LRRTM1 underlies synaptic convergence in visual thalamus** *eLife* **7** https://doi.org/10.7554/eLife.33498 | PubMed | Google Scholar

12. Hong YK, Park S, Litvina EY, Morales J, Sanes JR, Chen C (2014) **Refinement of the retinogeniculate synapse by bouton clustering** *Neuron* **84**:332–9 https://doi.org/10.1016/j.neuron.2014.08.059 | PubMed | Google Scholar

13. Mason CA (1982) **Development of terminal arbors of retino-geniculate axons in the kitten--I. Light microscopical observations** *Neuroscience* **7**:541–59 https://doi.org/10.1016/0306-4522(82)90063-x | PubMed | Google Scholar

14. Hamos JE, Van Horn SC, Raczkowski D, Sherman SM (1987) **Synaptic circuits involving an individual retinogeniculate axon in the cat** *J Comp Neurol* **259**:165–92 https://doi.org/10.1002/cne.902590202 | PubMed | Google Scholar

15. Hammer S, Monavarfeshani A, Lemon T, Su J, Fox MA (2015) **Multiple Retinal Axons Converge onto Relay Cells in the Adult Mouse Thalamus** *Cell Rep* **12**:1575–83 https://doi.org/10.1016/j.celrep.2015.08.003 | PubMed | Google Scholar

16. Morgan JL, Berger DR, Wetzel AW, Lichtman JW (2016) **The Fuzzy Logic of Network Connectivity in Mouse Visual Thalamus** *Cell* **165**:192–206 https://doi.org/10.1016/j.cell.2016.02.033 | PubMed | Google Scholar

17. Budisantoso T, Matsui K, Kamasawa N, Fukazawa Y, Shigemoto R (2012) **Mechanisms Underlying Signal Filtering at a Multisynapse Contact** *J Neurosci* **32**:2357 https://doi.org/10.1523/JNEUROSCI.5243-11.2012 | Google Scholar

18. Sherman SM, Guillery RW (1998) **On the actions that one nerve cell can have on another: distinguishing "drivers" from "modulators"** *Proc Natl Acad Sci U S A* **95**:7121–6 https://doi.org/10.1073/pnas.95.12.7121 | PubMed | Google Scholar

19. Guillery RW, Sherman SM (2002) **Thalamic Relay Functions and Their Role in Corticocortical Communication: Generalizations from the Visual System** *Neuron* **33**:163–75 https://doi.org/10.1016/S0896-6273(01)00582-7 | Google Scholar

20. Sretavan D, Shatz CJ (1984) **Prenatal development of individual retinogeniculate axons during the period of segregation** *Nature* **308**:845–8 https://doi.org/10.1038/308845a0 | PubMed | Google Scholar

21. Sretavan DW, Shatz CJ (1986) **Prenatal development of retinal ganglion cell axons: segregation into eye-specific layers within the cat's lateral geniculate nucleus** *J Neurosci* **6**:234–51 https://doi.org/10.1523/JNEUROSCI.06-01-00234.1986 | PubMed | Google Scholar

22. Dhande OS, Hua EW, Guh E, Yeh J, Bhatt S, Zhang Y, Ruthazer ES, Feller MB, Crair MC (2011) **Development of single retinofugal axon arbors in normal and beta2 knock-out mice** *J Neurosci* **31**:3384–99 https://doi.org/10.1523/JNEUROSCI.4899-10.2011 | PubMed | Google Scholar

23. Campbell G, Shatz CJ (1992) **Synapses formed by identified retinogeniculate axons during the segregation of eye input** *J Neurosci* **12**:1847–58 https://doi.org/10.1523/JNEUROSCI.12-05-01847.1992 | PubMed | Google Scholar

24. Chen C, Regehr WG (2000) **Developmental remodeling of the retinogeniculate synapse** *Neuron* **28**:955–66 https://doi.org/10.1016/s0896-6273(00)00166-5 | PubMed | Google Scholar

25. Hauser JL, Liu X, Litvina EY, Chen C (2014) **Prolonged synaptic currents increase relay neuron firing at the developing retinogeniculate synapse** *J Neurophysiol* **112**:1714–28 https://doi.org/10.1152/jn.00451.2014 | PubMed | Google Scholar

26. Zhang C, Yadav S, Speer CM (2023) **The synaptic basis of activity-dependent eye-specific competition** *Cell Rep* **42**:112085 https://doi.org/10.1016/j.celrep.2023.112085 | PubMed | Google Scholar

27. Vatan T, Minehart JA, Zhang C, Agarwal V, Yang J, Speer CM (2021) **Volumetric super-resolution imaging by serial ultrasectioning and stochastic optical reconstruction**

microscopy in mouse neural tissue *STAR Protocols* **2**:100971 https://doi.org/10.1016/j.xpro.2021.100971 | Google Scholar

28. Muir-Robinson G, Hwang BJ, Feller MB (2002) **Retinogeniculate axons undergo eye-specific segregation in the absence of eye-specific layers** *J Neurosci* **22**:5259–64 https://doi.org/10.1523/jneurosci.22-13-05259.2002 | PubMed | Google Scholar

29. Xu HP, Burbridge TJ, Chen MG, Ge X, Zhang Y, Zhou ZJ, Crair MC (2015) **Spatial pattern of spontaneous retinal waves instructs retinotopic map refinement more than activity frequency** *Dev Neurobiol* **75**:621–40 https://doi.org/10.1002/dneu.22288 | PubMed | Google Scholar

30. Xu HP, Furman M, Mineur YS, Chen H, King SL, Zenisek D, Zhou ZJ, Butts DA, Tian N, Picciotto MR, Crair MC (2011) **An instructive role for patterned spontaneous retinal activity in mouse visual map development** *Neuron* **70**:1115–27 https://doi.org/10.1016/j.neuron.2011.04.028 | PubMed | Google Scholar

31. Xu HP, Burbridge TJ, Ye M, Chen M, Ge X, Zhou ZJ, Crair MC (2016) **Retinal Wave Patterns Are Governed by Mutual Excitation among Starburst Amacrine Cells and Drive the Refinement and Maintenance of Visual Circuits** *J Neurosci* **36**:3871–86 https://doi.org/10.1523/JNEUROSCI.3549-15.2016 | PubMed | Google Scholar

32. Rossi FM, Pizzorusso T, Porciatti V, Marubio LM, Maffei L, Changeux JP (2001) **Requirement of the nicotinic acetylcholine receptor beta 2 subunit for the anatomical and functional development of the visual system** *Proc Natl Acad Sci U S A* **98**:6453–8 https://doi.org/10.1073/pnas.101120998 | PubMed | Google Scholar

33. Grubb MS, Rossi FM, Changeux JP, Thompson ID (2003) **Abnormal functional organization in the dorsal lateral geniculate nucleus of mice lacking the beta 2 subunit of the nicotinic acetylcholine receptor** *Neuron* **40**:1161–72 https://doi.org/10.1016/s0896-6273(03)00789-x | PubMed | Google Scholar

34. Sun C, Warland DK, Ballesteros JM, van der List D, Chalupa LM (2008) **Retinal waves in mice lacking the beta2 subunit of the nicotinic acetylcholine receptor** *Proc Natl Acad Sci U S A* **105**:13638–43 https://doi.org/10.1073/pnas.0807178105 | PubMed | Google Scholar

35. Stafford BK, Sher A, Litke AM, Feldheim DA (2009) **Spatial-temporal patterns of retinal waves underlying activity-dependent refinement of retinofugal projections** *Neuron* **64**:200–12 https://doi.org/10.1016/j.neuron.2009.09.021 | PubMed | Google Scholar

36. Bansal A, Singer JH, Hwang BJ, Xu W, Beaudet A, Feller MB (2000) **Mice lacking specific nicotinic acetylcholine receptor subunits exhibit dramatically altered spontaneous activity patterns and reveal a limited role for retinal waves in forming ON and OFF circuits in the inner retina** *J Neurosci* **20**:7672–81 https://doi.org/10.1523/jneurosci.20-20-07672.2000 | PubMed | Google Scholar

37. Hammer S, Carrillo GL, Govindaiah G, Monavarfeshani A, Bircher JS, Su J, Guido W, Fox MA (2014) **Nuclei-specific differences in nerve terminal distribution, morphology, and development in mouse visual thalamus** *Neural Dev* **9** https://doi.org/10.1186/1749-8104-9-16 | PubMed | Google Scholar

38. Zhang Q, Lee WA, Paul DL, Ginty DD (2019) **Multiplexed peroxidase-based electron microscopy labeling enables simultaneous visualization of multiple cell types** *Nat Neurosci* **22**:828–39 https://doi.org/10.1038/s41593-019-0358-7 | PubMed | Google Scholar

39. Koch SM, Dela Cruz CG, Hnasko TS, Edwards RH, Huberman AD, Ullian EM (2011) **Pathway-specific genetic attenuation of glutamate release alters select features of competition-based visual circuit refinement** *Neuron* **71**:235–42 https://doi.org/10.1016/j.neuron.2011.05.045 | PubMed | Google Scholar

40. Su J, Byer L, Liang Y, Fox MA (2024) **Distribution, development, and identity of retinal ganglion cells labeled in the Sert-Cre reporter mouse** *Journal of Comparative Neurology* **532**:e25606 https://doi.org/10.1002/cne.25606 | Google Scholar

41. Johnson KP, Fitzpatrick MJ, Zhao L, Wang B, McCracken S, Williams PR, Kerschensteiner D (2021) **Cell-type-specific binocular vision guides predation in mice** *Neuron* **109**:1527–39 https://doi.org/10.1016/j.neuron.2021.03.010 | PubMed | Google Scholar

42. Assali A, Gaspar P, Rebsam A (2014) **Activity dependent mechanisms of visual map formation--from retinal waves to molecular regulators** *Semin Cell Dev Biol* **35**:136–46 https://doi.org/10.1016/j.semcdb.2014.08.008 | PubMed | Google Scholar

43. Fassier C, Nicol X (2021) **Retinal Axon Interplay for Binocular Mapping** *Front Neural Circuits* **15** https://doi.org/10.3389/fncir.2021.679440 | PubMed | Google Scholar

44. Penn AA, Riquelme PA, Feller MB, Shatz CJ (1998) **Competition in retinogeniculate patterning driven by spontaneous activity** *Science* **279**:2108–12 https://doi.org/10.1126/science.279.5359.2108 | PubMed | Google Scholar

45. Assali A, Le Magueresse C, Bennis M, Nicol X, Gaspar P, Rebsam A (2017) **RIM1/2 in retinal ganglion cells are required for the refinement of ipsilateral axons and eye-specific segregation** *Sci Rep* **7**:3236 https://doi.org/10.1038/s41598-017-03361-0 | PubMed | Google Scholar

46. Fredj NB, Hammond S, Otsuna H, Chien C-B, Burrone J, Meyer MP (2010) **Synaptic Activity and Activity-Dependent Competition Regulates Axon Arbor Maturation, Growth Arrest, and Territory in the Retinotectal Projection** *J Neurosci* **30**:10939 https://doi.org/10.1523/JNEUROSCI.1556-10.2010 | Google Scholar

47. Hua JY, Smear MC, Baier H, Smith SJ (2005) **Regulation of axon growth in vivo by activity-based competition** *Nature* **434**:1022–6 https://doi.org/10.1038/nature03409 | PubMed | Google Scholar

48. Rahman TN, Munz M, Kutsarova E, Bilash OM, Ruthazer ES (2020) **Stentian structural plasticity in the developing visual system** *Proc Natl Acad Sci U S A* **117**:10636–8 https://doi.org/10.1073/pnas.2001107117 | PubMed | Google Scholar

49. Munz M, Gobert D, Schohl A, Poquérusse J, Podgorski K, Spratt P, Ruthazer ES (2014) **Rapid Hebbian axonal remodeling mediated by visual stimulation** *Science* **344**:904–9 https://doi.org/10.1126/science.1251593 | PubMed | Google Scholar

50. Zhang LI, Tao HW, Holt CE, Harris WA (1998) **A critical window for cooperation and competition among developing retinotectal synapses** *Nature* **395**:37–44 https://doi.org/10.1038/25665 | Google Scholar

51. Matsumoto N, Barson D, Liang L, Crair MC (2024) **Hebbian instruction of axonal connectivity by endogenous correlated spontaneous activity** *Science* **385**:eadh7814 https://doi.org/10.1126/science.adh7814 | PubMed | Google Scholar

52. Yasuda M, Nagappan-Chettiar S, Johnson-Venkatesh EM, Umemori H (2021) **An activity-dependent determinant of synapse elimination in the mammalian brain** *Neuron* **109**:1333–49 https://doi.org/10.1016/j.neuron.2021.03.006 | PubMed | Google Scholar

53. Louail A, Sierksma MC, Chaffiol A, Baudet S, Assali A, Couvet S, Nedjam M, Roche F, Zagar Y, Duebel J, Nicol X (2020) **cAMP-Dependent Co-stabilization of Axonal Arbors from Adjacent Developing Neurons** *Cell Rep* **33**:108220 https://doi.org/10.1016/j.celrep.2020.108220 | PubMed | Google Scholar

54. Kutsarova E, Schohl A, Munz M, Wang A, Zhang YY, Bilash OM, Ruthazer ES (2023) **BDNF signaling in correlation-dependent structural plasticity in the developing visual system** *PLoS Biol* **21**:e3002070 https://doi.org/10.1371/journal.pbio.3002070 | PubMed | Google Scholar

55. Godement P, Salaün J, Imbert M (1984) **Prenatal and postnatal development of retinogeniculate and retinocollicular projections in the mouse** *J Comp Neurol* **230**:552–75 https://doi.org/10.1002/cne.902300406 | PubMed | Google Scholar

56. Mooney R, Madison DV, Shatz CJ (1993) **Enhancement of transmission at the developing retinogeniculate synapse** *Neuron* **10**:815–25 https://doi.org/10.1016/0896-6273(93)90198-z | PubMed | Google Scholar

57. Ziburkus J, Dilger EK, Lo FS, Guido W (2009) **LTD and LTP at the developing retinogeniculate synapse** *J Neurophysiol* **102**:3082–90 https://doi.org/10.1152/jn.90618.2008 | PubMed | Google Scholar

58. Butts DA, Kanold PO, Shatz CJ (2007) **A burst-based "Hebbian" learning rule at retinogeniculate synapses links retinal waves to activity-dependent refinement** *PLoS Biol* **5**:e61 https://doi.org/10.1371/journal.pbio.0050061 | PubMed | Google Scholar

59. Lee H, Brott BK, Kirkby LA, Adelson JD, Cheng S, Feller MB, Datwani A, Shatz CJ (2014) **Synapse elimination and learning rules co-regulated by MHC class I H2-Db** *Nature* **509**:195–200 https://doi.org/10.1038/nature13154 | PubMed | Google Scholar

60. Chung WS, Clarke LE, Wang GX, Stafford BK, Sher A, Chakraborty C, Joung J, Foo LC, Thompson A, Chen C, Smith SJ, Barres BA (2013) **Astrocytes mediate synapse elimination through MEGF10 and MERTK pathways** *Nature* **504**:394–400 https://doi.org/10.1038/nature12776 | PubMed | Google Scholar

61. Stevens B, Allen NJ, Vazquez LE, Howell GR, Christopherson KS, Nouri N, Micheva KD, Mehalow AK, Huberman AD, Stafford B, Sher A, Litke AM, Lambris JD, Smith SJ, John SW, Barres BA (2007) **The classical complement cascade mediates CNS synapse elimination** *Cell* **131**:1164–78 https://doi.org/10.1016/j.cell.2007.10.036 | PubMed | Google Scholar

62. Schafer DP, Lehrman EK, Kautzman AG, Koyama R, Mardinly AR, Yamasaki R, Ransohoff RM, Greenberg ME, Barres BA, Stevens B (2012) **Microglia sculpt postnatal neural circuits in an activity and complement-dependent manner** *Neuron* **74**:691–705 https://doi.org/10.1016/j.neuron.2012.03.026 | PubMed | Google Scholar

63. Hooks BM, Chen C (2006) **Distinct roles for spontaneous and visual activity in remodeling of the retinogeniculate synapse** *Neuron* **52**:281–91 https://doi.org/10.1016/j.neuron.2006.07.007 | PubMed | Google Scholar

64. Dilger EK, Krahe TE, Morhardt DR, Seabrook TA, Shin HS, Guido W (2015) **Absence of plateau potentials in dLGN cells leads to a breakdown in retinogeniculate refinement** *J Neurosci* **35**:3652–62 https://doi.org/10.1523/jneurosci.2343-14.2015 | PubMed | Google Scholar

65. Cork RJ, Namkung Y, Shin HS, Mize RR (2001) **Development of the visual pathway is disrupted in mice with a targeted disruption of the calcium channel beta(3)-subunit gene** *J Comp Neurol* **440**:177–91 https://doi.org/10.1002/cne.1378 | PubMed | Google Scholar

66. Fernández-Nogales M, López-Cascales MT, Murcia-Belmonte V, Escalante A, Fernández-Albert J, Muñoz-Viana R, Barco A, Herrera E (2022) **Multiomic Analysis of Neurons with Divergent Projection Patterns Identifies Novel Regulators of Axon Pathfinding** *Adv Sci (Weinh)* **9**:e2200615 https://doi.org/10.1002/advs.202200615 | PubMed | Google Scholar

67. Wang Q, Marcucci F, Cerullo I (2016) **Mason C. Ipsilateral and Contralateral Retinal Ganglion Cells Express Distinct Genes during Decussation at the Optic Chiasm** *eneuro* **3**:ENEURO.0169-16.2016 https://doi.org/10.1523/ENEURO.0169-16.2016 | Google Scholar

68. Nicol X, Voyatzis S, Muzerelle A, Narboux-Nême N, Südhof TC, Miles R, Gaspar P (2007) **cAMP oscillations and retinal activity are permissive for ephrin signaling during the establishment of the retinotopic map** *Nat Neurosci* **10**:340–7 https://doi.org/10.1038/nn1842 | PubMed | Google Scholar

69. Balice-Gordon RJ, Chua CK, Nelson CC, Lichtman JW (1993) **Gradual loss of synaptic cartels precedes axon withdrawal at developing neuromuscular junctions** *Neuron* **11**:801–15 https://doi.org/10.1016/0896-6273(93)90110-d | PubMed | Google Scholar

70. Gan WB, Lichtman JW (1998) **Synaptic segregation at the developing neuromuscular junction** *Science* **282**:1508–11 https://doi.org/10.1126/science.282.5393.1508 | PubMed | Google Scholar

71. Wyatt RM, Balice-Gordon RJ (2003) **Activity-dependent elimination of neuromuscular synapses** *J Neurocytol* **32**:777–94 https://doi.org/10.1023/b:Neur.0000020623.62043.33 | PubMed | Google Scholar

72. Chen J, Mizushige T, Nishimune H (2012) **Active zone density is conserved during synaptic growth but impaired in aged mice** *J Comp Neurol* **520**:434–52 https://doi.org/10.1002/cne.22764 | PubMed | Google Scholar

73. Balice-Gordon RJ, Lichtman JW (1994) **Long-term synapse loss induced by focal blockade of postsynaptic receptors** *Nature* **372**:519–24 https://doi.org/10.1038/372519a0 | PubMed | Google Scholar

74. Buffelli M, Burgess RW, Feng G, Lobe CG, Lichtman JW, Sanes JR (2003) **Genetic evidence that relative synaptic efficacy biases the outcome of synaptic competition** *Nature* **424**:430–4 https://doi.org/10.1038/nature01844 | PubMed | Google Scholar

75. Kopp DM, Perkel DJ, Balice-Gordon RJ (2000) **Disparity in neurotransmitter release probability among competing inputs during neuromuscular synapse elimination** *J Neurosci* **20**:8771–9 https://doi.org/10.1523/jneurosci.20-23-08771.2000 | PubMed | Google Scholar

76. Sanes JR, Lichtman JW (1999) **Development of the vertebrate neuromuscular junction** *Annu Rev Neurosci* **22**:389–442 https://doi.org/10.1146/annurev.neuro.22.1.389 | PubMed | Google Scholar

77. Misgeld T, Kummer TT, Lichtman JW, Sanes JR (2005) **Agrin promotes synaptic differentiation by counteracting an inhibitory effect of neurotransmitter** *Proc Natl Acad Sci USA* **102**:11088–93 https://doi.org/10.1073/pnas.0504806102 | Google Scholar

78. Lin W, Dominguez B, Yang J, Aryal P, Brandon EP, Gage FH, Lee KF (2005) **Neurotransmitter acetylcholine negatively regulates neuromuscular synapse formation by a Cdk5-dependent mechanism** *Neuron* **46**:569–79 https://doi.org/10.1016/j.neuron.2005.04.002 | PubMed | Google Scholar

79. Hashimoto K, Kano M (2013) **Synapse elimination in the developing cerebellum** *Cell Mol Life Sci* **70**:4667–80 https://doi.org/10.1007/s00018-013-1405-2 | PubMed | Google Scholar

80. Bosman LW, Konnerth A (2009) **Activity-dependent plasticity of developing climbing fiber-Purkinje cell synapses** *Neuroscience* **162**:612–23 https://doi.org/10.1016/j.neuroscience.2009.01.032 | PubMed | Google Scholar

81. Hashimoto K, Kano M (2003) **Functional differentiation of multiple climbing fiber inputs during synapse elimination in the developing cerebellum** *Neuron* **38**:785–96 https://doi.org/10.1016/s0896-6273(03)00298-8 | PubMed | Google Scholar

82. Nitta A, Yamasaki M, Miyazaki T, Konno K, Yoshimura H, Watanabe M (2025) **Molecular and Anatomical Strengthening of "Winner" Climbing Fiber Synapses in Developing Mouse Purkinje Cells** *J Neurosci* https://doi.org/10.1523/JNEUROSCI.2156-24.2025 | PubMed | Google Scholar

83. Wilson AM, Schalek R, Suissa-Peleg A, Jones TR, Knowles-Barley S, Pfister H, Lichtman JW (2019) **Developmental Rewiring between Cerebellar Climbing Fibers and Purkinje Cells Begins with Positive Feedback Synapse Addition** *Cell Rep* **29**:2849–61 https://doi.org/10.1016/j.celrep.2019.10.081 | Google Scholar

84. Bosman LWJ, Takechi H, Hartmann J, Eilers J, Konnerth A (2008) **Homosynaptic Long-Term Synaptic Potentiation of the "Winner" Climbing Fiber Synapse in Developing Purkinje Cells** *J Neurosci* **28**:798 https://doi.org/10.1523/JNEUROSCI.4074-07.2008 | Google Scholar

85. Ohtsuki G, Hirano T (2008) **Bidirectional plasticity at developing climbing fiber-Purkinje neuron synapses** *Eur J Neurosci* **28**:2393–400 https://doi.org/10.1111/j.1460-9568.2008.06539.x | PubMed | Google Scholar

86. Lorenzetto E, Caselli L, Feng G, Yuan W, Nerbonne JM, Sanes JR, Buffelli M (2009) **Genetic perturbation of postsynaptic activity regulates synapse elimination in developing cerebellum** *Proc Natl Acad Sci USA* **106**:16475–80 https://doi.org/10.1073/pnas.0907298106 | Google Scholar

87. Kawamura Y, Nakayama H, Hashimoto K, Sakimura K, Kitamura K, Kano M (2013) **Spike timing-dependent selective strengthening of single climbing fibre inputs to Purkinje cells during cerebellar development** *Nat Commun* **4**:2732 https://doi.org/10.1038/ncomms3732 | Google Scholar

88. Benninger K, Hood G, Simmel D, Tuite L, Wetzel A, Ropelewski A, Watkins S, Watson A, Bruchez M (2020) **Cyberinfrastructure of a Multi-Petabyte Microscopy Resource for Neuroscience Research** In: *Practice and Experience in Advanced Research Computing* Portland, OR, USA: Association for Computing Machinery pp. 1–7 Google Scholar

89. Paxinos G (2007) **Atlas of the developing mouse brain at E17.5, P0 and P6** Amsterdam; Boston: Elsevier :353 Google Scholar

90. Babcock H, Sigal YM, Zhuang X (2012) **A high-density 3D localization algorithm for stochastic optical reconstruction microscopy** *Optical Nanoscopy* **1** https://doi.org/10.1186/2192-2853-1-6 | Google Scholar

91. Babcock HP, Huang F, Speer CM (2019) **Correcting Artifacts in Single Molecule Localization Microscopy Analysis Arising from Pixel Quantum Efficiency Differences in sCMOS Cameras** *Sci Rep* **9**:18058 https://doi.org/10.1038/s41598-019-53698-x | PubMed | Google Scholar

Zhang C, Yadav S, Speer CM (2023) **The synaptic basis of activity-dependent eye-specific competition** *Brain Image Library* https://doi.org/10.35077/g.1164

Author information

Chenghang Zhang
Department of Biology, University of Maryland, College Park, College Park, United States 20742
ORCID iD: 0000-0003-1346-2186

Tarlan Vatan
Department of Biology, University of Maryland, College Park, College Park, United States 20742

Colenso M Speer
Department of Biology, University of Maryland, College Park, College Park, United States 20742
ORCID iD: 0000-0002-3076-7072

For correspondence: cspeer@umd.edu

Editors

Reviewing Editor
Marla Feller
University of California, Berkeley, Berkeley, United States of America

Senior Editor
Panayiota Poirazi
FORTH Institute of Molecular Biology and Biotechnology, Heraklion, Greece

Joint Public Review:

Summary:

The authors previously published a study of RGC boutons in the dLGN in developing wild-type mice and developing mutant mice with disrupted spontaneous activity. In the current manuscript, they have broken down their analysis of RGC boutons according to the number of Homer/Bassoon puncta associated with each vGlut3 cluster.

The authors find that, in the first post-natal week, RGC boutons with multiple active zones (mAZs) are about a third as common as boutons with a single active zone (sAZ). The size of the vGluT2 cluster associated with each bouton was proportional to the number of active zones present in each bouton. Within the author's ability to estimate these values (n=3 per group, 95% of results expected to be within ~2.5 standard deviations), these results are consistent across groups: 1) dominant eye vs. non-dominant eye, 2) wild-type mice vs. mice with activity blocked, and at 3) ages P2, P4, and P8. The authors also found that mAZs and sAZs also have roughly the same number (about 1.5) of sAZs clustered around them (within 1.5 um).

There has been much discussion with the reviewers through multiple versions of this paper. of how to interpret these findings. Based on a large number of tests for statistical significance, the authors interpreted the presence of a statistical significance difference as evidence that "Eye-specific active zone clustering underlies synaptic competition in the developing visual system (title of previous version of manuscript)". The reviewers have focused on the small effect size as indicating that the small differences observed are not informative regarding this biological question. The authors have now tempered this interpretation.

Strengths:

The source dataset is high resolution data showing the colocalization of multiple synaptic proteins across development. Added to this data is labeling that distinguishes axons from the right eye from axons from the left eye. The first order analysis of this data showing changes in synapse density and in the occurrence of multi-active zone synapses is useful information about the development of an important model for activity dependent synaptic remodeling.

Reviewing Editor's comment on the latest revision (without sending the paper back to the individual reviewers):

In their latest revision, the authors have moderated earlier causal claims, incorporated additional statistical controls, and largely maintained their original interpretation of the data. While these changes address some prior concerns, the underlying issues remain. The previous review emphasized that the reported effect sizes were small and therefore hard to link to biological relevance. The authors argue that the effect sizes are large. Given the lack of a biological argument for this effect size, this point is really semantic. We would like to point out that the effect size measurement the authors used is likely a standard effect size calculation (the difference between groups is divided by the standard deviation of the groups). With only three experiments and irregular variance, it is likely that their estimates of standard deviation-and therefore effect size-are unreliable. Overall, the revisions improve presentation but do not substantively resolve the difficulty in drawing strong conclusions from the data set raised earlier.

https://doi.org/10.7554/eLife.91431.4.sa1

Author response:

The following is the authors' response to the previous reviews

> ***Reviewer #1 (Public review):***
>
> *Summary*
>
> *The authors previously published a study of RGC boutons in the dLGN in developing wild-type mice and developing mutant mice with disrupted spontaneous activity. In the*

> *current manuscript, they have broken down their analysis of RGC boutons according to the number of Homer/Bassoon puncta associated with each vGlut3 cluster.*
>
> *The authors find that, in the first post-natal week, RGC boutons with multiple active zones (mAZs) are about a third as common as boutons with a single active zone (sAZ). The size of the vGluT2 cluster associated with each bouton was proportional to the number of active zones present in each bouton. Within the author's ability to estimate these values (n=3 per group, 95% of results expected to be within ~2.5 standard deviations), these results are consistent across groups: 1) dominant eye vs. nondominant eye, 2) wild-type mice vs. mice with activity blocked, and at 3) ages P2, P4, and P8. The authors also found that mAZs and sAZs also have roughly the same number (about 1.5) of sAZs clustered around them (within 1.5 um).*
>
> *However, the authors do not interpret this consistency between groups as evidence that active zone clustering is not a specific marker or driver of activity dependent synaptic segregation. Rather, the authors perform a large number of tests for statistical significance and cite the presence or absence of statistical significance as evidence that "Eye-specific active zone clustering underlies synaptic competition in the developing visual system (title)". I don't believe this conclusion is supported by the evidence.*

We have revised the title to be descriptive: "Eye-specific differences in active zone addition during synaptic competition in the developing visual system." While our correlative approach does not establish direct causality, our findings provide important structural evidence that complements existing functional studies of activity-dependent synaptic refinement. We have carefully revised the text throughout to avoid causal language, focusing instead on the developmental patterns we observe.

> *Strengths*
>
> *The source dataset is high resolution data showing the colocalization of multiple synaptic proteins across development. Added to this data is labeling that distinguishes axons from the right eye from axons from the left eye. The first order analysis of this data showing changes in synapse density and in the occurrence of multi-active zone synapses is useful information about the development of an important model for activity dependent synaptic remodeling.*
>
> *Weaknesses*
>
> *In my previous review I argued that it was not possible to determine, from their analysis, whether the differences they were reporting between groups was important to the biology of the system. The authors have made some changes to their statistics (paired t-tests) and use some less derived measures of clustering. However, they still fail to present a meaningfully quantitative argument that the observed group differences are important. The authors base most of their claims on small differences between groups. There are two big problems with this practice. First, the differences between groups appear too small to be biologically important. Second, the differences between groups that are used as evidence for how the biology works are generally smaller than the precision of the author's sampling. That is, the differences are as likely to be false positives as true positives.*
>
> *(1) Effect size. The title claims: "Eye-specific active zone clustering underlies synaptic competition in the developing visual system". Such a claim might be supported if the authors found that mAZs are only found in dominant-eye RGCs and that eye-specific segregation doesn't begin until some threshold of mAZ frequency is reached. Instead, the behavior of mAZs is roughly the same across all conditions. For example, the clear trend in Figure 4C and D is that measures of clustering between mAZ and sAZ are as similar as*

> *could reasonably be expected by the experimental design. However, some of the comparisons of very similar values produced p-values < 0.05. The authors use this fact to argue that the negligible differences between mAZ and sAZs explain the development of the dramatic differences in the distribution of ipsilateral and contralateral RGCs.*

We have changed the title to avoid implying a causal relationship between clustering and eye-specific segregation. Our key findings in Figures 4C and 4D demonstrate effect sizes >2.0 with high statistical power (Supplemental Table S2). While the absolute magnitude of differences is modest (5-7%), these high effect sizes combined with low inter-animal variability demonstrate consistent, reproducible biological phenomena. During development, small differences during critical periods can have profound downstream consequences for synaptic refinement outcomes.

We acknowledge that significance in Figure 4 arises due to low variance between biological replicates rather than large mean differences. We have revised the text to describe these as "slight" differences and that "WT mice show a tendency toward forming more synapses near mAZ inputs," reflecting appropriate caution in our interpretation while maintaining the statistical robustness of our findings.

> *(2) Sample size. Performing a large number of significance tests and comparing pvalues is not hypothesis testing and is not descriptive science. At best, with large sample sizes and controls for multiple tests, this approach could be considered exploratory. With n=3 for each group, many comparisons of many derived measures, among many groups, and no control for multiple testing, this approach constitutes a random result generator.*
>
> *The authors argue that n=3 is a large sample size for the type of high resolution / large volume data being used. It is true that many electron microscopy studies with n=1 are used to reveal the patterns of organization that are possible within an individual. However, such studies cannot control individual variation and are, therefore, not appropriate for identifying subtle differences between groups.*
>
> *In response to previous critiques along these lines, the authors argue they have dealt with this issue by limiting their analysis to within-individual paired comparisons. There are several problems with their thinking in this approach. The main problem is that they did not change the logic of their arguments, only which direction they pointed the t-tests. Instead of claiming that two groups are different because p < 0.05, they say that two groups are different because one produced p < 0.05 and the other produced p > 0.05. These arguments are not statistically valid or biologically meaningful.*

We have implemented rigorous statistical controls, applying false discovery rate (FDR) correction using the Benjamini-Hochberg method ($\alpha = 0.05$) within each experimental condition (age × genotype combination). This correction strategy treats each condition as addressing a distinct experimental question: “What synaptic properties differ between left eye and right eye inputs in this specific developmental stage and genotype?” The approach appropriately controls for multiple testing while preserving power to detect biologically meaningful differences. We applied FDR correction separately to the ~20-34 measurements (varying by age and genotype) within each of the six experimental conditions, resulting in condition-specific adjusted p-values reported in updated Supplemental Table S2. This correction confirmed the robustness of our key findings. We do not base conclusions solely on comparing p-values across conditions. Our interpretations focus on effect sizes, confidence intervals, and consistent patterns within each condition, with statistical significance providing supporting evidence rather than the primary basis for biological conclusions.

> *To the best of my understanding, the results are consistent with the following model:*

RGCs form mAZs at large boutons (known)

About a quarter of week-one RGC boutons are mAZs (new observation)

Vesicle clustering is proportional to active zone number (~new observation)

RGC synapse density increases during the first post-week (known)

Blocking activity reduces synapse density (known)

Contralateral eye RGCs for more and larger synapses in the lateral dLGN (known)

While mAZ formation is known in adult and juvenile dLGN, the formation of mAZ boutons during eye-specific competition represents new information with important functional implications. Synapses with multiple release sites should be stronger than single-active-zone synapses, suggesting a structural correlate for competitive advantage during refinement.

We demonstrate distinct developmental patterns for sAZ versus mAZ contacts during the first postnatal week. Multi-active zone density favors the dominant eye, while single active-zone synapse density from the competing eye increases from P2-P4 to match dominant-eye levels. This reveals that newly formed synapses from the competing eye predominantly contain single release sites, marking P4-P8 as a critical window for understanding molecular mechanisms driving synaptic elimination.

Our results show that altered retinal activity patterns (β2KO mice) reduce synapse density during eye-specific competition. We relied on β2 knockout mice, which retain retinal waves and spontaneous spike activity but with disrupted patterns and output levels compared to controls. We make no claims about complete activity blockade. Previous studies using different activity manipulations (epibatidine, TTX) have examined terminal morphology, but effects on synapse density during competition remain largely unknown. Achieving complete retinal activity blockade is technically challenging, making it of interest to revisit the role of activity using more precise manipulations to control spike output and relative timing.

With n=3 and effect sizes smaller than 1 standard deviation, a statistically significant result is about as likely to be a false positive as a true positive.

A true-positive statistically significant result does is not evidence of a meaningful deviation from a biological model.

Our conclusions are based on results with effect sizes substantially larger than 1. Key findings demonstrate effect sizes exceeding 2.0. These large effect sizes, combined with rigorous FDR correction and low inter-animal variability, provide evidence against false positive results. During critical developmental periods, consistent structural differences, even those modest in absolute magnitude, can reflect important regulatory mechanisms that influence refinement outcomes. All statistical results, effect sizes, and power analyses are reported in Supplementary Tables S2, with confidence intervals in Supplementary Table S3. We have revised the text in several places where small differences are presented to reflect appropriate caution in our interpretation.

Providing plots that show the number of active zones present in boutons across these various conditions is useful. However, I could find no compelling deviation from the above default predictions that would influence how I see the role of mAZs in activity dependent eye-specific segregation.

Below are critiques of most of the claims of the manuscript.

> *Claim (abstract): individual retinogeniculate boutons begin forming multiple nearby presynaptic active zones during the first postnatal week.*
>
> *Confirmed by data.*
>
> *Claim (abstract): the dominant-eye forms more numerous mAZ contacts,*
>
> *Misleading: The dominant-eye (by definition) forms more contacts than the nondominant eye. That includes mAZ.*

While the dominant eye forms more total contacts, the pattern depends critically on contact type and developmental stage. The dominant eye forms more mAZ contacts across all ages (Figures 2 and S1). However, for sAZ contacts, the two eyes form similar numbers at P4, with the non-dominant eye showing increased sAZ formation during this critical period. This differential pattern by synapse type represents an important aspect of how synaptic competition unfolds structurally.

> *Claim (abstract): At the height of competition, the non-dominant-eye projection adds many single active zone (sAZ) synapses*
>
> *Weak: While the individual observation is strong, it is a surprising deviation based on a single n=3 experiment in a study that performed twelve such experiments (six ages, mutant/wildtype, sAZ/mAZ)*

The difference in eye-specific sAZ formation at P2 and P8 had effect sizes of ~5.3 and ~2.7 respectively (after FDR correction the difference was still significant at P2 and trending at P8). At P4, no effect was observed by paired T-test and the 5/95% confidence intervals ranged from -0.021-0.008 synapses/μm^3. The consistency of this pattern across P2 and P8, combined with the large effect sizes, supports the reliability of this developmental finding. We report all effect sizes and power test analyses in Supplemental Table S2, and confidence intervals in Supplemental Table S3.

> *Claim (abstract): Together, these findings reveal eye-specific differences in release site addition during synaptic competition in circuits essential for visual perception and behavior.*
>
> *False: This claim is unambiguously false. The above findings, even if true, do not argue for any functional significance to active zone clustering.*

Our phrasing “circuits essential for visual perception and behavior” referred to the general importance of binocular organization in the retinogeniculate system for visual processing and we did not intend to claim direct functional significance of our structural data. For clarity we have deleted the latter part of this sentence. In lines 35-37, the abstract now reads “Together, these findings reveal eye-specific differences in release site addition that correlate with axonal refinement outcomes during retinogeniculate refinement.”

> *Claim (line 84): "At the peak of synaptic competition midway through the first postnatal week, the non-dominant-eye formed numerous sAZ inputs, equalizing the global synapse density between the two eyes"*
>
> *Weak: At one of twelve measures (age, bouton type, genotype) performed with 3 mice each, one density measure was about twice as high as expected.*

The difference in eye-specific sAZ formation at P2 and P8 had effect sizes of ~5.3 and ~2.7 respectively (after FDR correction the difference was still significant at P2 and trending at

P8). At P4, no effect was observed by paired T-test and the 5/95% confidence intervals ranged from -0.021-0.008 synapses/□m^3. The consistency of this pattern across P2 and P8, combined with the large effect sizes, supports the reliability of this developmental finding. We report all effect sizes and power test analyses in Supplemental Table S2, and confidence intervals in Supplemental Table S3.

> *Claim (line 172): "In WT mice, both mAZ (Fig. 3A, left) and sAZ (Fig. 3B, left) inputs showed significant eye-specific volume differences at each age."*
>
> *Questionable: There appears to be a trend, but the size and consistency is unclear.*
>
> *Claim (line 175): "the median VGluT2 cluster volume in dominant-eye mAZ inputs was 3.72 fold larger than that of non-dominant-eye inputs (Fig. 3A, left)."*
>
> *Cherry picking. Twelve differences were measured with an n of 3, 3 each time. The biggest difference of the group was cited. No analysis is provided for the range of uncertainty about this measure (2.5 standard deviations) as an individual sample or as one of twelve comparisons.*
>
> *Claim (line 174): "In the middle of eye-specific competition at P4 in WT mice, the median VGluT2 cluster volume in dominant-eye mAZ inputs was 3.72 fold larger than that of non-dominant-eye inputs (Fig. 3A, left). In contrast, β2KO mice showed a smaller 1.1 fold difference at the same age (Fig. 3A, right panel). For sAZ synapses at P4, the magnitudes of eye-specific differences in VGluT2 volume were smaller: 1.35-fold in WT (Fig. 3B, left) and 0.41-fold in β2KO mice (Fig. 3B, right). Thus, both mAZ and sAZ input size favors the dominant eye, with larger eye-specific differences seen in WT mice (see Table S3)."*
>
> *No way to judge the reliability of the analysis and trivial conclusion: To analyze effect size the authors choose the median value of three measures (whatever the middle value is). They then make four comparisons at the time point where they observed the biggest difference in favor of their hypothesis. There is no way to determine how much we should trust these numbers besides spending time with the mislabeled scatter plots. The authors then claim that this analysis provides evidence that there is a difference in vGluT2 cluster volume between dominant and non-dominant RGCs and that that difference is activity dependent. The conclusion that dominant axons have bigger boutons and that mutants that lack the property that would drive segregation would show less of a difference is very consistent with the literature. Moreover, there is no context provided about what 1.35 or 1.1 fold difference means for the biology of the system.*

We focused on P4 for biological reasons rather than post-hoc selection. P4 represents the established peak of synaptic competition when eye-specific synapse densities are globally equivalent. This is a timepoint consistently highlighted throughout our manuscript and supported by previous literature. We have modified our presentation from fold changes to measured eye-specific differences in volume (mean ± standard error) and added confidence intervals in Supplemental Table S3. The effect sizes for eye-specific differences in VGluT2 volume at P4 are robust: ~2.3 and ~1.5 for mAZ and sAZ measurements in WT mice, and ~2.5 and ~1.8 in β2KO mice, with all analyses well-powered (Supplemental Table S2).

We were unable to identify any mislabeled scatter plots and believe all figures are correctly labeled. While dominant-eye advantage in bouton size is consistent with previous literature, our study provides the first detailed analysis of how this develops specifically during the critical period of competition, with distinct patterns for single versus multi-active zone contacts. Our data show that dominant-eye inputs have larger vesicle pools that scale with active zone number. While this suggests enhanced transmission capacity, we make no direct physiological claims based on structural data alone.

> *Claim (189): "This shows that vesicle docking at release sites favors the dominant-eye as we previously reported but is similar for like eye type inputs regardless of AZ number."*
>
> *Contradicts core claim of manuscript: Consistent with previous literature, there is an activity dependent relative increase in vGlut2 clustering of dominant eye RGCs. The new information is that that activity dependence is more or less the same in sAZ and mAZ. The only plausible alternative is that vGlut2 scaling only increases in mAZ which would be consistent with the claims of their paper. That is not what they found. To the extent that the analysis presented in this manuscript tests a hypothesis, this is it. The claim of the title has been refuted by figure 3.*

We report the volume of docked vesicle signal (VGluT2) nearby each active zone, finding this is greater for dominant-eye synapses. Within each eye-specific synapse population, vesicle signal per active zone is similar regardless of whether these are part of single- or multi-active zone contacts. This is consistent with a modular program of active zone assembly and maintenance: core molecular programs facilitate docking at each AZ similarly regardless of how many AZs are nearby.

This finding does not contradict our main conclusions but rather provides insight into how synaptic advantages are structured. The dominant eye's advantage may arise in part from forming more multi-AZ contacts (which have proportionally more docked vesicles) rather than from enhanced vesicle loading per individual active zone. This organization may reflect how developmental competition operates through contact number and active zone addition rather than fundamental changes to individual release site properties.

We have changed the title to be descriptive rather than mechanistic.

> *Claim (line 235): "For the non-dominant eye projection, however, clustered mAZ inputs outnumbered clustered sAZ inputs at P4 (Fig. 4C, bottom left panel), the age when this eye adds sAZ synapses (Fig. 2C)."*
>
> *Misleading: The overwhelming trend across 24 comparisons is that the sAZ clustering looks like mAZ clustering. That is the objective and unambiguous result. Among these 24 underpowered tests (n=3), there were a few p-values < 0.05. The authors base their interpretation of cell behavior on these crossings.*

In Figures 4C and 4D we report significant results with high effect sizes (effect sizes all greater than 2; see Supplemental Table S2). The mean differences are modest (5-7%) and significance arises due to low variance between biological replicates. We acknowledge that clustering patterns are generally similar between mAZ and sAZ inputs across most conditions. We have revised the text to describe these as “slight” differences and that “WT mice show a tendency toward forming more synapses near mAZ inputs”, reflecting appropriate caution in our interpretation while noting the statistical consistency of these patterns.

> *Claim (line 328): "The failure to add synapses reduced synaptic clustering and more inputs formed in isolation in the mutants compared to controls."*
>
> *Trivially true: Density was lower in mutant.*

We have rewritten the sentence for clarity: “The failure to add synapses could explain the observation that synaptic clustering was reduced and more inputs formed in isolation in the mutants compared to controls.”

> *Claim (line 332): "While our findings support a role for spontaneous retinal activity in presynaptic release site addition and clustering..."*
>
> *Not meaningfully supported by evidence: I could not find meaningful differences between WT and mutant beside the already known dramatic difference in synapse density.*

We have changed the sentence to avoid overinterpreting the results. The new sentence in lines 415-417 reads: “While our results highlight developmental changes in presynaptic release site addition and clustering, activity-dependent postsynaptic mechanisms also influence input refinement at later stages.”

> ***Reviewer #2 (Public review):***
>
> *Summary:*
>
> *In this manuscript, Zhang and Speer examine changes in the spatial organization of synaptic proteins during eye specific segregation, a developmental period when axons from the two eyes initially mingle and gradually segregate into eye-specific regions of the dorsal lateral geniculate. The authors use STORM microscopy and immunostain presynaptic (VGluT2, Bassoon) and postsynaptic (Homer) proteins to identify synaptic release sites. Activity-dependent changes of this spatial organization are identified by comparing the β2KO mice to WT mice. They describe two types of synapses based on Bassoon clustering: the multiple active zone (mAZ) synapse and single active zone (sAZ) synapse. In this revision, the authors have added EM data to support the idea that mAZ synapses represent boutons with multiple release sites. They have also reanalyzed their data set with different statistical approaches.*
>
> *Strengths:*
>
> *The data presented is of good quality and provides an unprecedented view at high resolution of the presynaptic components of the retinogeniculate synapse during active developmental remodeling. This approach offers an advance to the previous mouse EM studies of this synapse because of the CTB label allows identification of the eye from which the presynaptic terminal arises.*
>
> *Weaknesses:*
>
> *While the interpretation of this data set is much more grounded in this second revised submission, some of the authors' conclusions/statements still lack convincing supporting evidence. In particular, the data does not support the title: "Eye-specific active zone clustering underlies synaptic competition in the developing visual system". The data show that there are fewer synapses made for both contra- and ipsi- inputs in the β2KO mice--this fact alone can account for the differences in clustering. There is no evidence linking clustering to synaptic competition. Moreover, the findings of differences in AZ# or distance between AZs that the authors report are quite small and it is not clear whether they are functionally meaningful.*

We thank the reviewer for their helpful suggestions that improved the manuscript in this revision. We have changed the title to remove the reference to “clustering” and to avoid implying any causal relationships. The new title is descriptive: “Eye-specific differences in active zone addition during synaptic competition in the developing visual system”.

To further address the reviewers comments, we have removed the remaining references to activity-dependent effects on synaptic development (line 36, line 96, line 415). We have also modified the text in lines 411-413 to state that “The failure to add synapses could explain the

observation that synaptic clustering was reduced and more inputs formed in isolation in the mutants compared to controls."

We have also updated our presentation of results for Figure 4 to ensure that we do not causally link clustering to synaptic competition. In Figures 4C and 4D we report significant results with high effect sizes (effect sizes all greater than 2; see Supplemental Table S2). The mean differences are modest (5-7%) and significance arises due to low variance between biological replicates. We acknowledge that clustering patterns are generally similar between mAZ and sAZ inputs across most conditions. We have revised the text to describe these as "slight" differences and that "WT mice show a tendency toward forming more synapses near mAZ inputs", reflecting appropriate caution in our interpretation while noting the statistical consistency of these patterns.

> ***Reviewer #3 (Public review):***
>
> *This study is a follow-up to a recent study of synaptic development based on a powerful data set that combines anterograde labeling, immunofluorescence labeling of synaptic proteins, and STORM imaging (Cell Reports, 2023). Specifically, they use anti-Vglut2 label to determine the size of the presynaptic structure (which they describe as the vesicle pool size), anti-Bassoon to label active zones with the resolution to count them, and anti-Homer to identify postsynaptic densities. Their previous study compared the detailed synaptic structure across the development of synapses made with contraprojecting vs. ipsi-projecting RGCs and compared this developmental profile with a mouse model with reduced retinal waves. In this study, they produce a new detailed analysis on the same data set in which they classify synapses into "multi-active zone" vs. "single-active zone" synapses and assess the number and spacing of these synapses. The authors use measurements to make conclusions about the role of retinal waves in the generation of same-eye synaptic clusters. The authors interpret these results as providing insight into how neural activity drives synapse maturation, the strength of their conclusions is not directly tested by their analysis.*
>
> *Strengths:*
>
> *This is a fantastic data set for describing the structural details of synapse development in a part of the brain undergoing activity-dependent synaptic rearrangements. The fact that they can differentiate the eye of origin is what makes this data set unique over previous structural work. The addition of example images from the EM dataset provides confidence in their categorization scheme.*
>
> *Weaknesses:*
>
> *Though the descriptions of single vs multi-active zone synapses are important and represent a significant advance, the authors continue to make unsupported conclusions regarding the biological processes driving these changes. Although this revision includes additional information about the populations tested and the tests conducted, the authors do not address the issue raised by previous reviews. Specifically, they provide no assessment of what effect size represents a biologically meaningful result. For example, a more appropriate title is "The distribution of eye-specific single vs multiactive zone is altered in mice with reduced spontaneous activity" rather than concluding that this difference in clustering is somehow related to synaptic competition. Of course, the authors are free to speculate, but many of the conclusions of the paper are not supported by their results.*

We appreciate the reviewer's helpful critique. We have changed the title to be descriptive and avoid implying causal relationships.

We have applied false discovery rate (FDR) correction using the Benjamini-Hochberg method with α = 0.05 within each experimental condition (age × genotype combination). The FDR correction treats each condition as addressing a distinct experimental question: 'What synaptic properties differ between left eye and right eye inputs in this specific developmental stage and genotype?'

This correction strategy is appropriate because: 1) we focus our statistical comparisons within each age/genotype; 2) each age-genotype combination represents a separate biological context where different synaptic properties between eye-of-origin may be relevant; and 3) this approach controls for multiple testing within each experimental question while maintaining statistical power to detect meaningful biological differences.

We applied FDR correction separately to the ~20-34 measurements (varying with age and genotype) within each of the six experimental conditions (P2-WT, P2-ß2, P4-WT, P4-ß2, P8-WT, P8-ß2), resulting in condition-specific adjusted p-values. These are reported in the updated Supplemental Table S2. Figures have been also been updated to reflect the FDR-adjusted values. Selected between-genotype comparisons are presented descriptively using 5/95% confidence intervals. This correction confirmed the robustness of our key findings.

With regard to the biological significance of effect sizes, our key findings demonstrate effect sizes >2.0, indicating robust effects. During critical developmental periods, consistent structural differences, even those modest in absolute magnitude, can reflect important regulatory mechanisms that influence refinement outcomes. The differences in synaptic organization we observe occur during the first postnatal week when eyespecific competition is active, suggesting these patterns may be relevant to understanding how structural advantages emerge during synaptic refinement.

> ***Reviewer #1 (Recommendations for the authors):***
>
> *I have tried to understand the analysis and biology of this manuscript as best I can. I believe the analytical approach taken is not reliable and I have explained why in my public comments. I don't believe this manuscript is unique in taking this approach. I have recently published a paper on how common this approach is and why it doesn't work. I don't want to give the impression that the problem with the analysis was that it was not computationally sophisticated enough or that you did not jump through a specific statistical hoop. If I strip out the arguments that depend on misinterpretations of p-values and -instead- look at the scatterplots, I come up with a very different view of the data than what is described in the paper.*
>
> *The information in the plots could be translated into a rigorous statistical analysis of estimated differences between groups given the uncertainties of the experimental design. I don't really think that analysis would be useful. I think it would have been enough to publish the plots and report your estimates of the number of active zones in RGCs during development. I don't see evidence of an additional effect.*

We appreciate the reviewer's helpful comments throughout the review process. Mean active zone numbers per mAZ contact are presented in Figure S2D/E. We look forward to further technical and computational advances that will help us increase our data acquisition throughput and sample sizes when designing future studies.

> ***Reviewer #2 (Recommendations for the authors):***
>
> *The authors should modify the title and other text to be more consistent with the data. There is no evidence that active zone clustering has any direct relationship to synaptic competition.*

We appreciate the reviewer's helpful suggestions to ensure appropriate language around causal effects. We have modified the title to accurately reflect the results: "Eyespecific differences in active zone addition during synaptic competition in the developing visual system." We have revised the text in the abstract, introduction, and results section for Figures 4 to be consistent with the data and not imply causality of synapse clustering on segregation phenotypes.

> ***Reviewer #3 (Recommendations for the authors):***
>
> *Change the title.*

We appreciate the reviewer's feedback throughout the review process. We have modified the title to accurately reflect the results: "Eye-specific differences in active zone addition during synaptic competition in the developing visual system."

https://doi.org/10.7554/eLife.91431.4.sa0